Ecological Indicators 156 (2023) 111193

Contents lists available at ScienceDirect

Ecological Indicators

journal homepage: www.elsevier.com/locate/ecolind

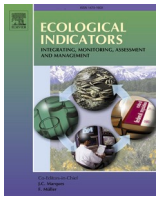

Original Articles

Rebound of surface and terrestrial water resources in Mongolian plateau following sustained depletion

Zhenfei Gao [a,b], Yan Zhou [a,b,*], Yaoping Cui [a,b,*], Jinwei Dong [c], Xinxin Wang [d], Guosong Zhao [e], Zhenhua Zou [f], Xiangming Xiao [g]

[a] Key Laboratory of Geospatial Technology for the Middle and Lower Yellow River Regions (Henan University), Ministry of Education, Kaifeng 475004, China
[b] College of Geography and Environmental Science, Henan University, Kaifeng 475004, China
[c] Key Laboratory of Land Surface Pattern and Simulation, Institute of Geographic Sciences and Natural Resources Research, Chinese Academy of Sciences, Beijing 100101, China
[d] Ministry of Education Key Laboratory for Biodiversity Science and Ecological Engineering, National Observations and Research Station for Wetland Ecosystems of the Yangtze Estuary, Institute of Biodiversity Science and Institute of Eco-Chongming, School of Life Sciences, Fudan University, Shanghai 200438, China
[e] Hubei Key Laboratory of Regional Ecology and Environmental Change, School of Geography and Information Engineering, China University of Geosciences, Wuhan 430074, China
[f] Department of Geographical Sciences, University of Maryland, College Park, MD 20742, USA
[g] Department of Microbiology and Plant Biology, University of Oklahoma, Norman, OK 73019, USA

ARTICLE INFO

Keywords:
Mongolian plateau
Surface water bodies
Terrestrial water storage
Google earth engine
Water resource recovery

ABSTRACT

Water resources have always played an important role in ensuring industrial and agricultural production, as well as maintaining ecosystem security in the Mongolian Plateau (MP), a typical arid to semi-arid region. Previous studies have reported the considerable shrinkages of surface water bodies affected by intense human disturbance in the MP before 2010. However, it is still unclear about the effects of those key ecological restoration efforts (e.g., the construction of ecological civilization since 2012) on water resources in the recent decade. Here, using all the available Landsat-5/7/8 surface reflectance observations, a robust water mapping algorithm based on spectral indices and thresholds, and the Google Earth Engine (GEE) cloud computing platform, we examined the changes in surface water area (SWA) in the MP during 1991–2021. In addition, based on the Gravity Recovery and Climate Experiment (GRACE) and GRACE Follow-On (GRACE-FO) Mascon data products, we investigated the inter-annual variability and trends of terrestrial water storage (TWS) from 2002 to 2021. We found that SWA experienced remarkable increases (85.5 km^2/yr) since 2009 after continuous shrinkage of surface water bodies (-205.9 km^2/yr) for over 20 years, in which Inner Mongolia played a dominant role in the recovery of SWA (72.2 km^2/yr). Also, TWS had undergone continuous decline before 2012 and fluctuating rebound after that. The most significant recovery of TWS mainly happened in the northern part of the MP. Quantitative attribution analyses showed that the key ecological restoration projects in China, especially the construction of ecological civilization since 2012, were the major drivers for the recovery of surface and terrestrial water resources. While previous studies reported the considerable decline of surface water resources induced by human activities in the MP since the 1990s, our research provided gratifying satellite evidence for the significant recoveries of surface and terrestrial water resources in the plateau during the past decade under the influence of ecological restoration efforts.

1. Introduction

Water resources are extremely critical for ensuring human life, agricultural and industrial production, as well as maintaining regional ecosystem stability and achieving sustainable development goals (SDGs) in the Mongolian Plateau (MP), which geographically includes Inner Mongolia in China and Mongolia and is a typical region with arid and semi-arid climate condition (Bao et al., 2019; Liu et al., 2022b). Surface

* Corresponding authors at: Key Laboratory of Geospatial Technology for the Middle and Lower Yellow River Regions (Henan University), Ministry of Education, Kaifeng 475004, China.
E-mail addresses: yanzhou@henu.edu.cn (Y. Zhou), cuiyp@lreis.ac.cn (Y. Cui).

https://doi.org/10.1016/j.ecolind.2023.111193
Received 31 July 2023; Received in revised form 9 October 2023; Accepted 29 October 2023
Available online 6 November 2023

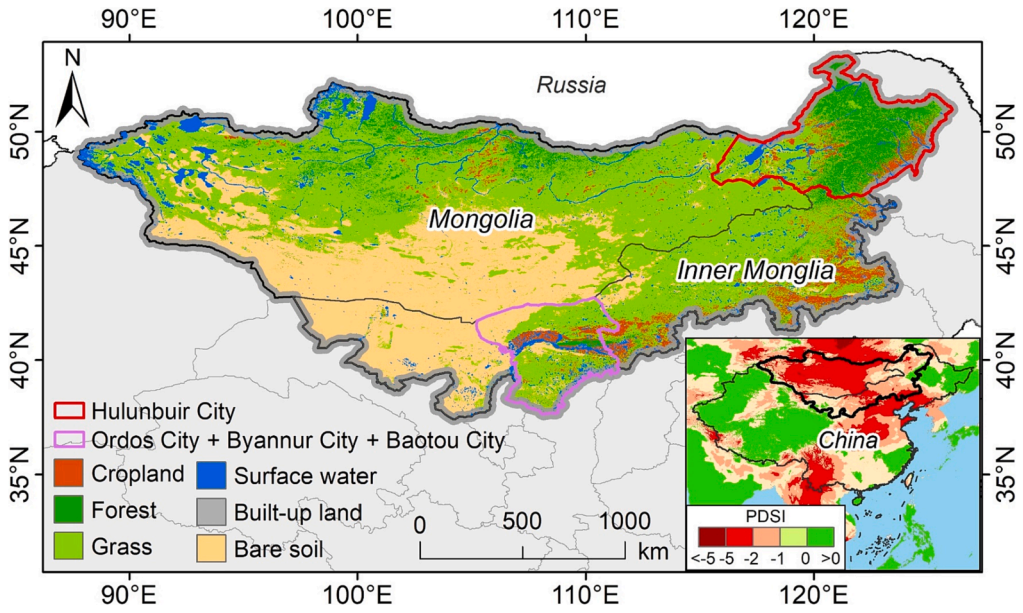

Fig. 1. Geographical location of the Mongolian Plateau (MP) and different land cover types within the region.

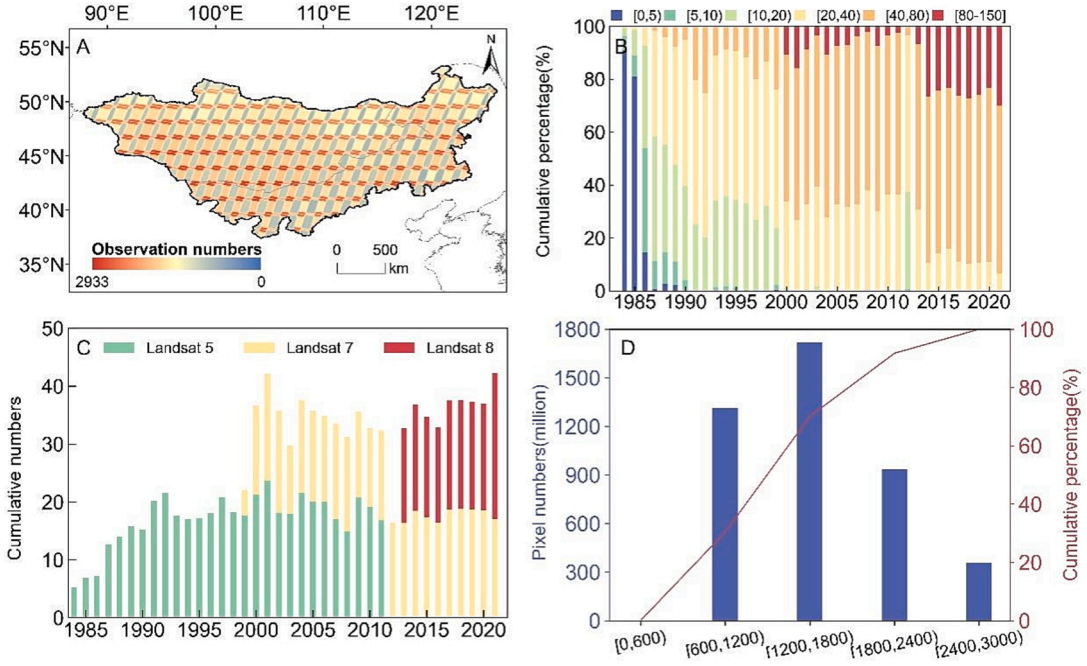

Fig. 2. Statistics of Landsat observation numbers in the MP. (A) Spatial distribution of the good-quality Landsat observation in the MP during 1984–2021. (B) Cumulative percentage of Landsat pixels with the good-quality observation numbers of [0,5), [5,10), [10,20), [20,40), [40,80), [80,150), respectively, in MP during 1984–2021. (C) The yearly average number of good-quality Landsat observations in MP during 1984–2021. (D) Number of Landsat pixels with the good-quality observation of [0,600), [600,1200), [1200,1800),[1800,2400), [2400,3000).

water area (SWA) and terrestrial water storage (TWS) are two crucial indicators of the overall status of regional water resources, which can be measured by different kinds of satellites in orbit. Previous studies (Tao et al., 2015; Zhou et al., 2019) had revealed the continuous decline of areas of surface water bodies mainly represented by these widely distributed lakes and wetlands in the whole MP from the late 1980s to around 2010, which was mainly caused by intense human disturbance (e.g., coal mining and overgrazing) and attracting much attention from governments and scientists. With the implementation of ecological civilization construction in China since 2012 (Wang et al., 2021), people's awareness of protecting ecology and the environment had strengthened, which might alleviate the deterioration of water resources in the MP. However, studies that focused on the dynamics of water resources in the MP from the both perspective of the areas of surface water bodies and total water storage are still limited so far, hindering our understanding of the completely changing processes of water resources. Therefore, updated and comprehensive pictures of the spatial patterns, long-term variations, and trends of SWA and TWS are extremely important for sustainable water management under anthropogenic disturbances and the earth's changing climate.

Surface water refers to these water bodies on the earth's surface, such as rivers, streams, lakes, reservoirs, wetlands, etc. They are always

Table 1
Confusion matrix for accuracy assessment of surface water maps in 1991, 2000, 2010, and 2020. The figures in the confusion matrices represent the total number of Landsat pixels.

1991				
Classification	Ground reference		Total	User accuracy
	Water	Non-water		
Water	9718	172	9890	98.26 %
Non-water	1032	23,478	24,510	95.79 %
Total	10,750	23,650	34,400	Overall accuracy = 96.5 %
Producer accuracy	90.4 %	99.27 %		Kappa Coefficient = 0.92
2000				
Classification	**Ground reference**		**Total**	**User accuracy**
	Water	**Non-water**		
Water	9030	516	9546	94.59 %
Non-water	559	24,295	24,854	97.75 %
Total	9589	24,811	34,400	Overall accuracy = 96.9 %
Producer accuracy	94.17 %	97.92 %		Kappa Coefficient = 0.92
2010				
Classification	**Ground reference**		**Total**	**User accuracy**
	Water	**Non-water**		
Water	8600	946	9,546	90.09 %
Non-water	344	24,510	24,854	98.62 %
Total	8944	25,456	34,400	Overall accuracy = 96.3 %
Producer accuracy	96.15 %	96.28 %		Kappa Coefficient = 0.90
2020				
Classification	**Ground reference**		**Total**	**User accuracy**
	Water	**Non-water**		
Water	8858	645	9503	93.21 %
Non-water	86	24,811	24,897	99.65 %
Total	8944	25,456	34,400	Overall accuracy = 97.9 %
Producer accuracy	99.04 %	97.47 %		Kappa Coefficient = 0.95

changing due to the combined effects of various natural and anthropogenic drivers (Ma et al., 2010; Zhu et al., 2020). With the rapid development of remote sensing technology, including the improvement of the spatial–temporal resolutions of satellite images and data processing capability, remote sensing has become more significant in measuring the dynamics of surface water bodies over large region scales with higher repeat frequencies (e.g., 8 days using time series Landsat observations) (Huang et al., 2018; Zou et al., 2018), especially in these distant mountainous areas (Zhang et al., 2017; Zhang et al., 2020a). Instead of traditional surveying methods, the more accurate and rapid extraction of surface water bodies based on remote sensing images has gradually become the mainstream approach and saved a lot of manpower and time (Chen and Zhao, 2022; Pekel et al., 2016; Song et al., 2018; Wu et al., 2023; Zou et al., 2017). In previous studies, various algorithms and remote sensing data sources have been used to extract surface water bodies, and their resultant single-period static maps have been released, such as the global water body data for 2000 with 30 m spatial resolution (Verpoorter et al., 2014) and for 2010 with 3 arc second resolution (Yamazaki et al., 2015). However, affected by the limitation of storing and processing massive remote sensing data, these static data products hinder our capability to precisely track the complete change processes of surface water bodies. Luckily, the development of cloud storage and cloud computing platforms (e.g., Google Earth Engine, GEE) promotes the emergence of time-series data products of surface water bodies, with the typical example of the 30 m global water body data set generated by the Joint Research Centre (JRC) in 2016 using all these Landsat top-of-atmosphere (TOA) reflectance data (Pekel et al., 2016). However, in this data set, there was a lack of surface water bodies in the MP before 2000. This is because the Landsat archive stored in the United States Geological Survey (USGS) Earth Resources Observation and Science (EROS) Center was dynamics due to the implementation of the Landsat Global Archive Consolidation (LGAC) effort which aimed to consolidate the Landsat data archives of all international ground stations to significantly increase the frequency of observations (Zhou et al., 2022; Zhu et al., 2019). Therefore, the Landsat archive might be less complete in 2016, when the JRC data was generated, than it was currently (Zhou et al., 2022).

Compared with TOA data, the Landsat surface reflectance (SR) data can eliminate the influence of the atmosphere and reflect the surface conditions more realistically (Dong et al., 2016), therefore, using SR data to extract surface water bodies would be more advantageous than TOA data. So far, there is no study based on the Landsat SR data to draw the annual map of all surface water bodies in the MP from the 1990 s to the present, which leads to the continuous monitoring of water resources in the MP being extremely limited. But now, a series of cloud computing platforms such as Google Earth Engine (GEE) were becoming more and more mature in technology, the improvement of data processing capabilities and the updated iteration of classification algorithms (Tamiminia et al., 2020), combined with the support of high-precision remote sensing images (e.g., Landsat SR data), had created good conditions for accurate identification of land cover types (Bian et al., 2020; Duan et al., 2020; Johnson, 2019; Liu et al., 2018). In previous studies, based on GEE and Landsat SR data, researchers had done some fruitful research on surface water dynamic changes at both national and regional scales (Wang et al., 2020; Zhou et al., 2022; Zou et al., 2018).

TWS is composed of all the detected or undetected water components on the earth, which is an important indicator of climate change. Traditional ways of detecting TWS were roughly estimated by manual measurement or hydrological model simulation, these methods were not only time-consuming and laborious but also limited by many factors and had low accuracy (Li et al., 2020a). The GRACE satellite is a satellite product jointly developed by the National Aeronautics and Space Administration (NASA) of the United States and the German Aeronautics Center and since its launch in March 2002, it has been widely used in research to monitor changes in TWS (Li et al., 2020a; Pokhrel et al., 2021; Wang et al., 2018; Zhao et al., 2021; Zhu et al., 2023). The evaluation of the water resources environment in the region based on gravity satellite data is the mainstream idea of current research, but this evaluation method was not comprehensive. Surface water is the main component of TWS (Wang et al., 2020), so the change of SWA could dominate the change of TWS (Getirana et al., 2017). However, up to now, the quantitative and comparative studies on the changes of SWA and TWS in the MP were very limited.

In this study, we intended to provide a holistic illustration of the continuous changes in SWA from 1991 to 2021 and TWS from 2002 to 2021 on the MP, and quantitatively analyze the driving forces of their changes. First of all, using all the available Landsat SR data, the water indices- and thresholds-based water mapping algorithm, and the GEE cloud computing platform, we generated the annual maps of year-long surface water bodies with a spatial resolution of 30 m in the MP. Secondly, we applied the GRACE and GRACE-FO mascon data sets to explore the spatial and temporal changes of TWS from 2002 to 2021. Finally, we qualitatively and quantitatively analyzed the drivers of changes in SWA and TWS by fully considering the effects of climate change and human activities. This study is expected to provide critical information for decision-makers and water managers who strive to

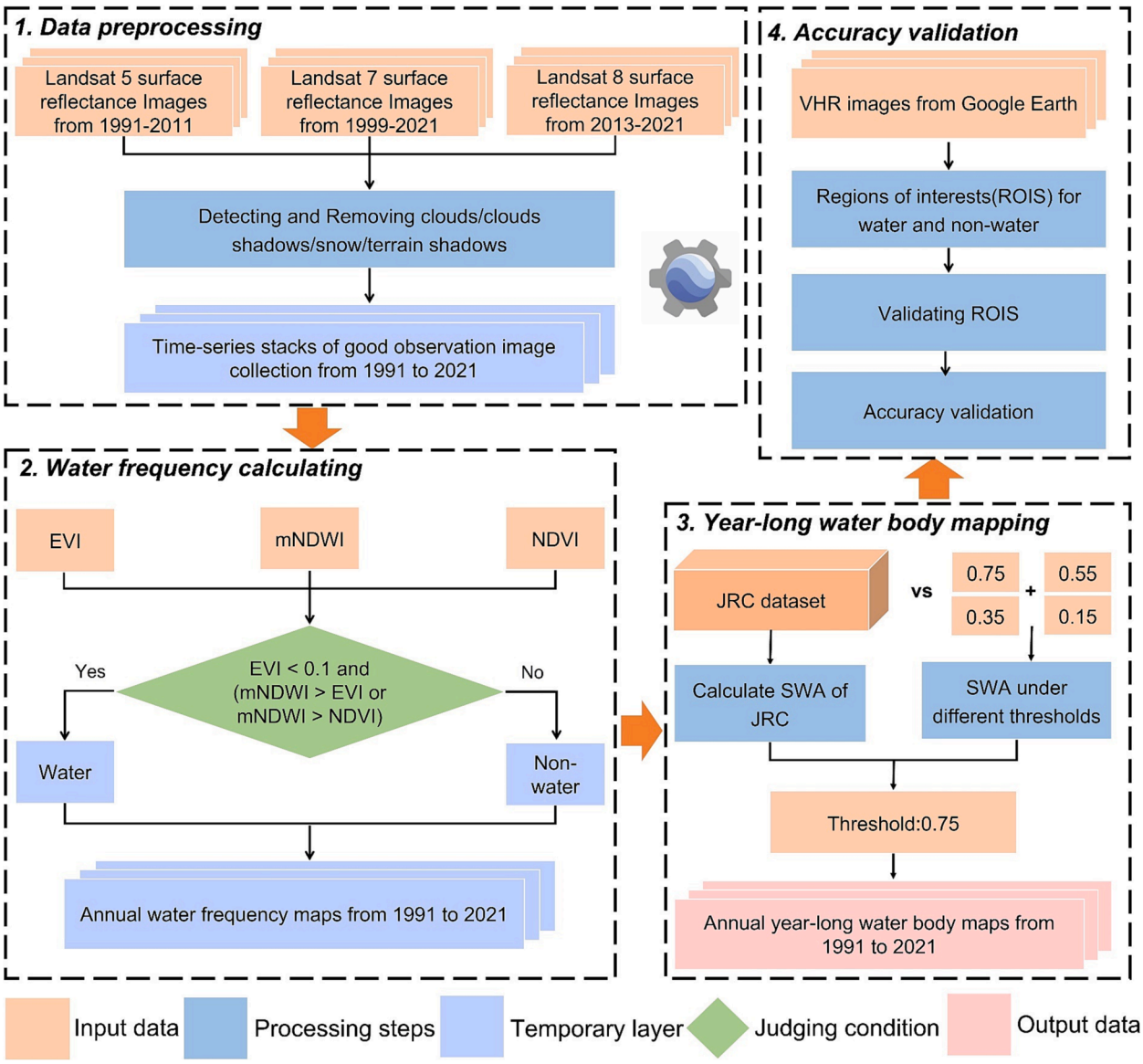

Fig. 3. Workflows for generating annual maps of year-long surface water bodies in the MP from 1991 to 2021.

achieve the coordinated development of water resource protection and social economy in the MP and offer a typical reference to analyze the changes of water resources in other similar regions around the world.

2. Materials and methods

2.1. Study area

The MP is in the inner Eurasian continent, mainly including the Inner Mongolia Autonomous Region in China and Mongolia (Fig. 1). The MP is rich in land cover types (John et al., 2013), of which grassland accounts for more than 50 % of its total areas (Qiang et al., 2019). It is a vital pasture area in Northern Asia for herding cattle and sheep, so pastoralism in the region is particularly developed and occupies a high proportion of the regional economic composition. Although the MP is a typical arid and semi-arid zone, there are still a large number of famous lakes (e.g., Lake Hulun in Inner Mongolia and Lake Hovsgol in Mongolia) and rivers (e.g., Yellow River in Inner Mongolia and Selenga River in Mongolia) with different sizes distributed in the region (Liu et al., 2022a; Wen et al., 2022). The sensitivity of MP to climate change determines that these surface water bodies in the region play an extremely important role in regulating internal ecological stability and ensuring people's production and living.

2.2. Data

2.2.1. Landsat imagery

As a widely used satellite data source for research related to geosciences, the Landsat archive has collected a large number of medium-resolution images through its family sensors (Loveland and Dwyer, 2012; Wulder et al., 2016). Among them, all these available 30-m resolution imagery from Landsat 5 (1984–2011), Landsat 7 (1999–2021), and Landsat 8 (2013–2021) were applied to the current research. These data stem from the United States Geological Survey (USGS) and can be obtained from the Google Earth Engine (https://earthengine.google.com), which provides multi-source geospatial data, advanced algorithms, and high-performance computing power to multidisciplinary research at different scales from regional to global (Amani et al., 2020; Gorelick et al., 2017). Compared to traditional image processing tools (e.g., ENVI), GEE can quickly batch process massive remote sensing images in a very short time. To verify the availability of the Landsat 5/7/8 Collection 1 Tier 1 SR image sets and determine the available time

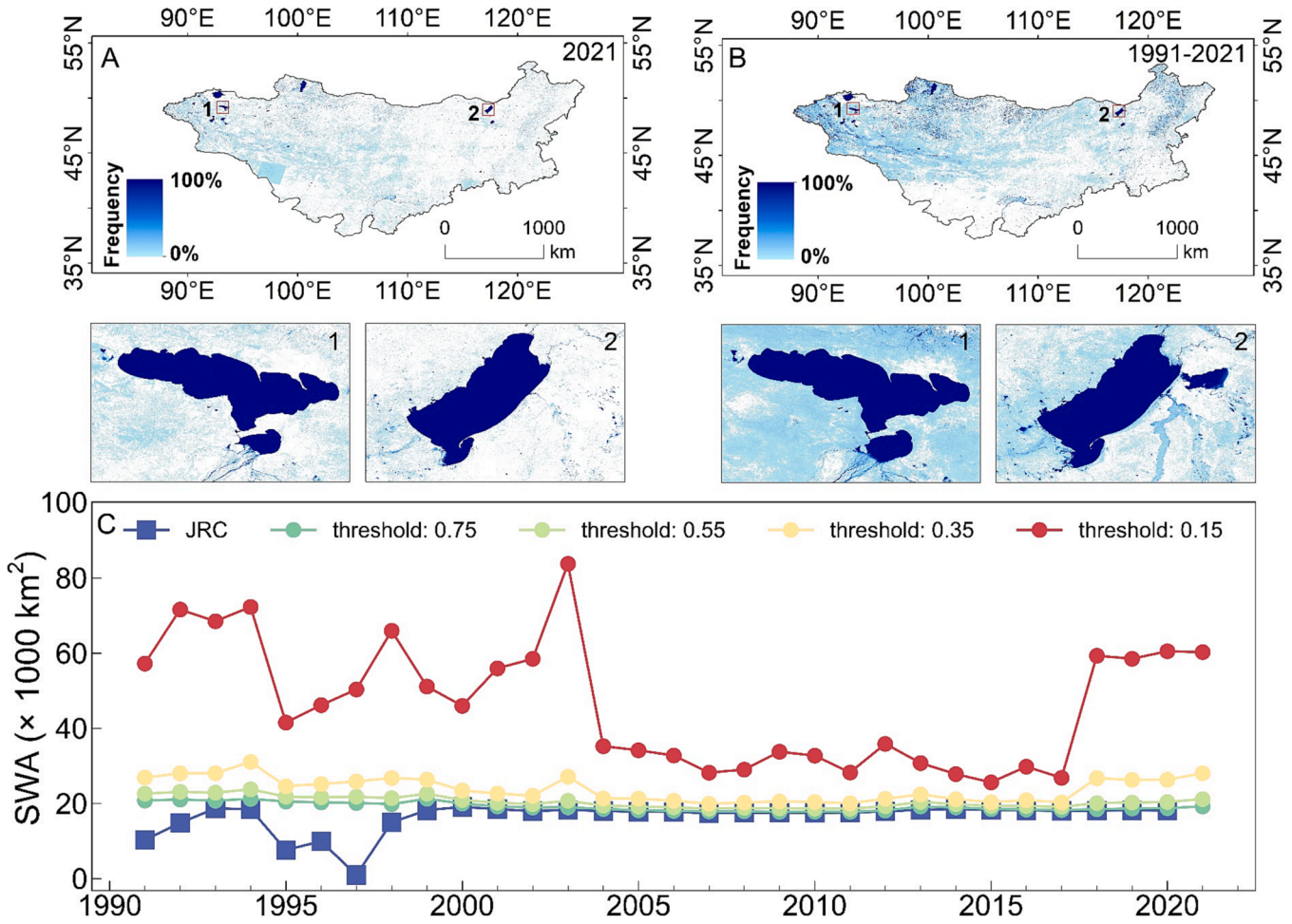

Fig. 4. Surface water frequency maps for the MP and changes in SWA under different thresholds. (A) Water frequency map in 2021; (B) Water frequency map during 1991–2021; The enlarged views below are lakes of Khyargas (1) and Hulun (2), respectively; (C) Annual areas of surface water bodies in the MP from 1991 to 2021 according to different frequency thresholds.

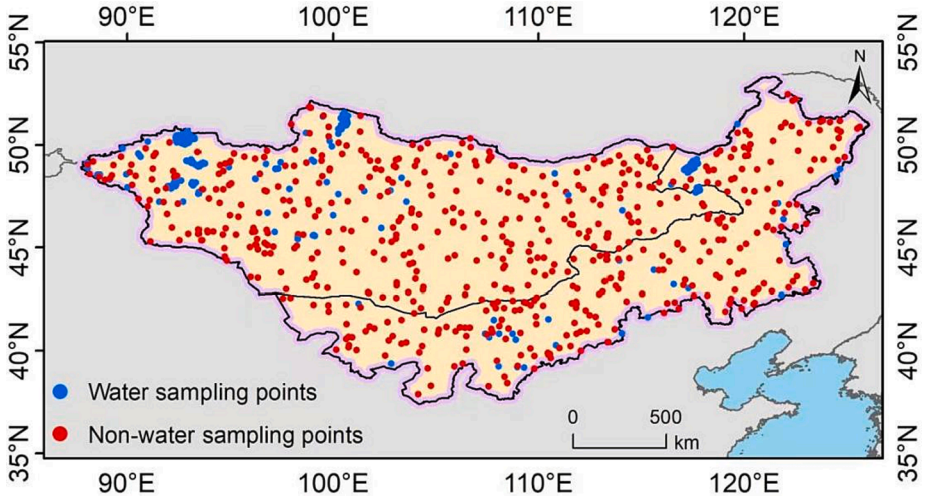

Fig. 5. Spatial distributions of the 800 areas of interest (AOIs) for accuracy assessment of these surface water maps for the MP.

interval for this study since the launch of the Landsat satellite in 1984, here, we have counted the annual numbers of good-quality Landsat observations in the MP from 1984 to 2021 by filtering those pixels of clouds, cloud shadows, snow, and terrain shadows. Among these bad-quality observations, clouds, cloud shadows, and snow were detected and removed using the quality assurance (QA) band in each image which was generated by the CFmask method (Foga et al., 2017). The terrain shadows were removed by using the combination of the two angles of solar azimuth, zenith, and digital elevation model (DEM) from the Shuttle Radar Topography Mission (SRTM) (Zhou et al., 2022). We

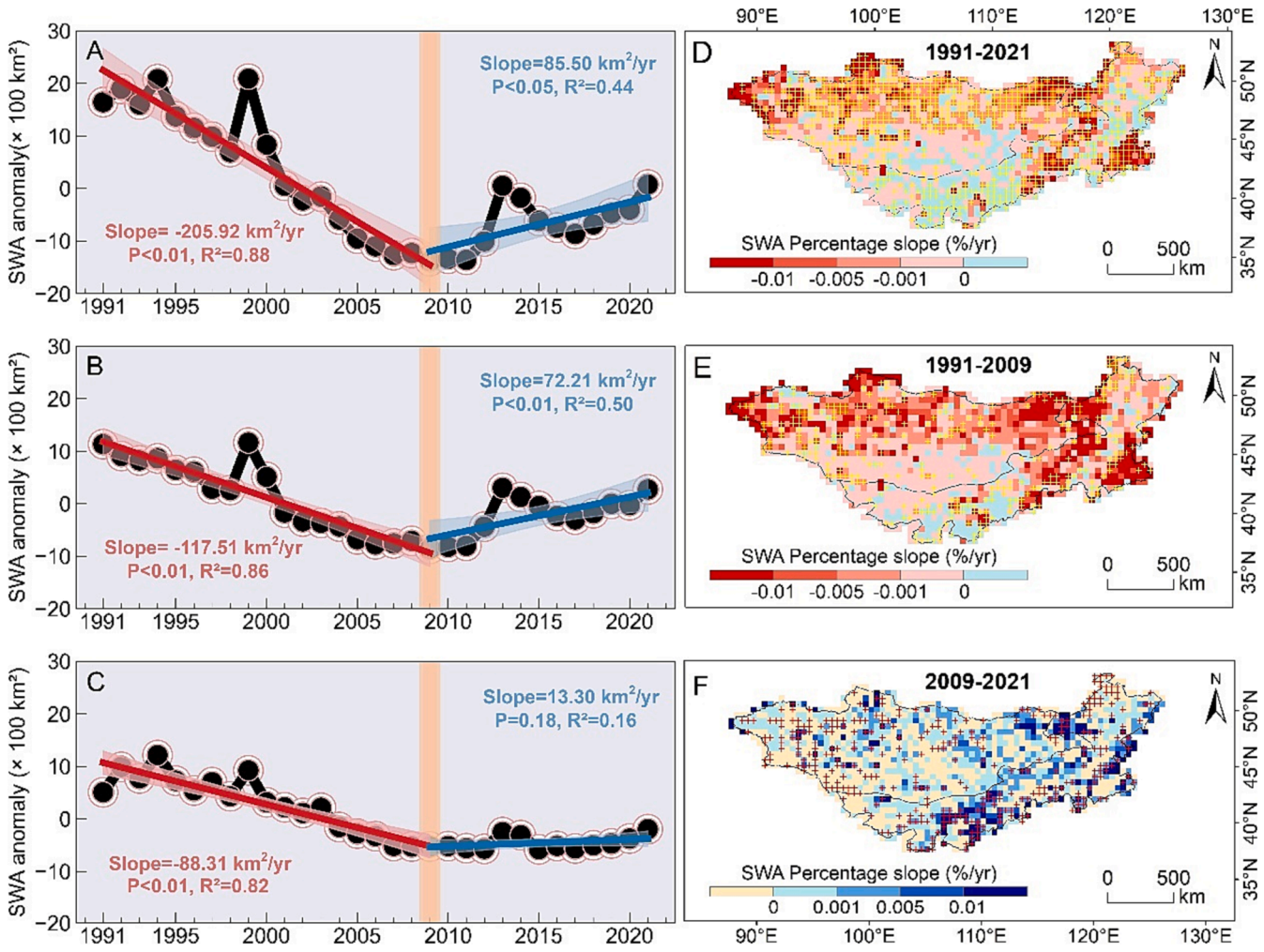

Fig. 6. Changes in SWA over the MP. Inter-annual variations and trends of SWA in the MP (A), Inner Mongolia (B), and Mongolia (C) from 1991 to 2021; Spatial patterns of linear trends of SWA in the MP during different periods of 1991–2021 (D), 1991–2009 (E), and 2009–2021 (F). The symbol "+" in each pixel indicated that the linear trends reached a statistical significance level of *p-value* < 0.05.

have conducted quantitative analyses on the availability of Landsat data to see whether there are sufficient good-quality Landsat observations to support retrospective and annual monitoring of surface water bodies on the MP since 1984. The results indicated that the Landsat pixels with zero good-quality observation in a year accounted for 24.5 % on average from 1984 to 1990. The insufficient good-quality Landsat observations restricted the generation of annual maps of surface water bodies on the MP before 1991. And there were enough good-quality Landsat observations to support conducting inter-annual monitoring of the dynamics of surface water bodies across the whole MP from 1991 to 2021, which was reflected by that the Landsat pixels with at least 10 good-quality observations annually accounted for over 99.9 % of the total pixels (Fig. 2). Therefore, we used all these Landsat 5/7/8 Collection 1 Tier 1 SR images (~180,000 images, ~ 176 TB) in the MP during 1991–2021 to examine the inter-annual variations and trends of SWA.

2.2.2. GRACE satellite data

The GRACE/GRACE Follow-On (GRACE-FO) Release-06 monthly mascon data products generated from NASA Jet Propulsion Laboratory (JPL) were used to track the inter-annual variations and trends of TWS in the MP during 2002–2021. The grid size and temporal resolution of these data sets are 0.5 arc degree and monthly. The GRACE/GRACE-FO mascon data provide a monthly gravity anomaly compared to the 2004–2010 time-average baseline, indicating the vertical mass deviation of water (Chambers et al., 2010; Chambers and Bonin, 2012). Considering that there were missing GRACE/GRACE-FO TWS values in some months, we applied a linear interpolation algorithm to fill the missing data according to the data of the previous and next months (Zhou et al., 2023). Then, the annual TWS anomalies of each grid were derived by averaging the GRACE/GRACE-FO values from the 12 months in each year.

2.2.3. Data on watershed extents and land covers

The watershed boundaries of the MP were derived from the HydroBASIN data product, which was developed by the World Wildlife Fund-US (WWF) (Lehner and Grill, 2013). The HydroBASIN follows the Pfafstetter codes concept and provides the boundaries of global watersheds from Level 1 to Level 12. In this study, we used the Level 5 watershed boundary data of HydroBASIN which divided the whole MP into 117 drainage basins to compare and analyze the changing trends of SWA and TWS at the watershed scale of MP. The GlobalLand 30 data product with 30-m resolution was used to examine the spatial patterns of different kinds of land covers in the MP. It has three editions of data in 2000, 2010, and 2020, including the first-level land cover types of cropland, forest, grassland, and water bodies, etc. (Jun et al., 2014). The global land cover data set was produced using multi-source remote sensing data, including satellite imagery from Landsat family sensors (i.e., TM, ETM+, and OLI) and China Environmental Disaster Reduction Satellite (HJ-1). In addition, the 2020 version of the data also used GF-1 multi-spectral images with a spatial resolution of 16 m. This paper used

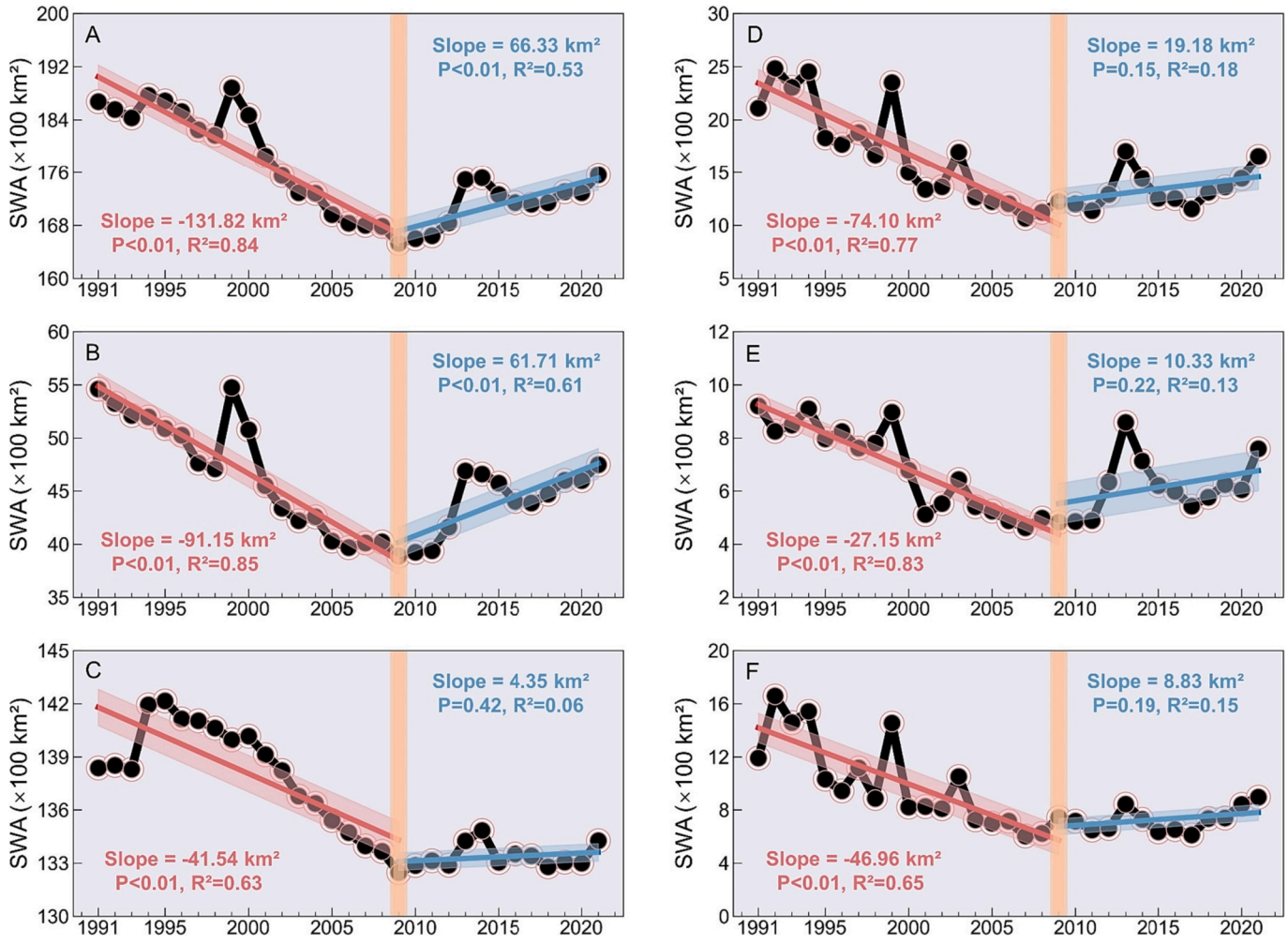

Fig.7. Inter-annual variabilities of surface water bodies with varying sizes in the MP from 1991 to 2021. Inter-annual variations and trends of large (≥1 km^2) water bodies in the MP (A), Inner Mongolia (B), and Mongolia (C) from 1991 to 2021. Inter-annual variations and trends of small (<1 km^2) water bodies in the MP (D), Inner Mongolia (E), and Mongolia (F) from 1991 to 2021.

the data of Edition 2020 of GlobalLand 30 to investigate the spatial distribution of major land cover types in the study area.

2.2.4. Climatic data

The annual mean temperature (AMT) and annual precipitation (AP) are two climate-driving factors that may have potential impacts on regional water resources (e.g. the increase in AMT will affect the rate of surface evapotranspiration, thereby accelerating the consumption of water resources) (Condon et al., 2020; Gbetkom et al., 2023). Two kinds of climatic data sets were used to examine the changes in AP and AMT, namely: the TerraClimate and the fifth-generation European Centre for Medium-Range Weather Forecasts (ECMWF) atmospheric reanalysis (ERA5). The TerraClimate is a global and monthly climatic dataset with a spatial resolution of 0.5 arc degree and it used climatically aided interpolation, with most of the information of temperature, precipitation, and water vapor pressure inherited from CRU Ts4.0 and the Japanese 55-year Reanalysis (JRA55) (Abatzoglou et al., 2018; Harris et al., 2020). The ERA5 data set provides hourly estimates of atmospheric, terrestrial, and marine climate variables, compared with previous products, ERA5 has greatly improved in resolution, number of variables, and other aspects, and is now selected by more researchers (Hongyuan et al., 2021). To reduce the uncertainties, we used the average of the two climatic data sets to investigate the trends of AP and AMT in the MP from 1991 to 2021.

2.3. Method

2.3.1. Generation of Landsat-based surface water maps

This study used the indices- and threshold-based automated water mapping algorithm to detect surface water bodies in satellite images. The main indexes in the algorithm include the modified Normalized Difference Water Index (mNDWI), Enhanced Vegetation Index (EVI), and Normalized Difference Vegetation Index (NDVI). The following equations introduced the calculations of the above indices using different spectral bands:

$$\mathrm{mNDWI} = \frac{\rho_{Green} - \rho_{SWIR1}}{\rho_{Green} + \rho_{SWIR1}} \quad (1)$$

$$\mathrm{NDVI} = \frac{\rho_{NIR} - \rho_{Red}}{\rho_{NIR} + \rho_{Red}} \quad (2)$$

$$\mathrm{EVI} = 2.5 \times \frac{\rho_{\mathrm{NIR}} - \rho_{\mathrm{Red}}}{1.0 + \rho_{\mathrm{NIR}} + 6.0\rho_{\mathrm{Red}} + 7.5\rho_{\mathrm{Blue}}} \quad (3)$$

where ρ_{red}, ρ_{green}, ρ_{Blue}, ρ_{NIR}, ρ_{SWIR1} are the surface reflectance of the bands of red, green, blue, near-infrared, and shortwave-infrared-1 (SWIR1) in Landsat imagery. According to our previous studies (Wang et al., 2020; Zhou et al., 2022; Zou et al., 2018), the rule mNDWI > NDVI or mNDWI > NDVI can be used to filter those pixels with stronger water signals than vegetation ones, while EVI < 0.1 can remove those pixels of

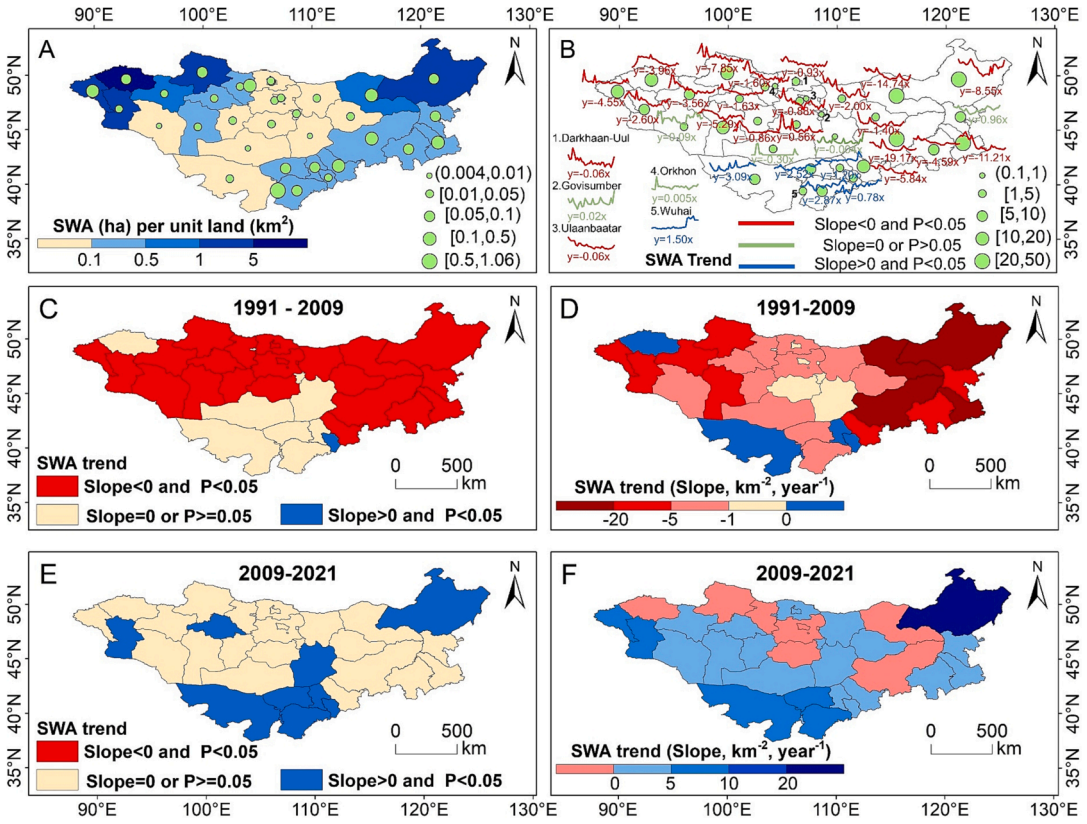

Fig. 8. Trends of SWA in the MP at the scale of the administrative region. (A) Annual mean SWA (ha) per unit land (km^2) and the standard deviation from 1991 to 2021; (B) Inter-annual variations and linear trends of SWA from 1991 to 2021; (C-D) Spatial patterns of linear trends of SWA from 1991 to 2009; (E-F) Spatial patterns of linear trends of SWA from 2009 to 2021.

vegetation and the mixes of water and vegetation. Therefore, we used Eq. (4) which introduced the relationships between the water and vegetation indices to identify if a given pixel was water or not.

$$\text{EVI} < 0.1 \text{ and } (\text{mNDWI} > \text{NDVI or mNDWI} > \text{EVI}) \quad (4)$$

After that, the frequency of water occurrence for a given pixel in one certain year was calculated using the following equation:

$$W_F = \frac{\sum_{i=1}^{N} W_i}{N} \times 100\% \quad (5)$$

where N represents the number of Landsat observations with good quality in the current year; W_i denotes whether the target pixel was surface water for the i-th observation, with "0" indicating non-water and "1" indicating water; W_F is the water frequency of the target pixel in that year. According to the above principles, we generated the annual frequency maps of surface water occurrence in the MP from 1991 to 2021. Fig. 4A and B showed the spatial distributions of water occurrence frequencies in the MP in 2021 and 1991–2021. Annual areas of surface water bodies greatly varied under different water frequency thresholds. To determine the most appropriate water frequency threshold for extracting year-long surface water bodies, we compared annual areas of surface water bodies according to different thresholds with the areas of year-long surface water bodies from the JRC data set (Fig. 4C), and found that annual areas of surface water bodies with the frequencies higher than or equal to 0.75 in our data set were the closest to the results from JRC data product. Therefore, we applied the threshold of 0.75 to separate year-long water bodies from annual water frequency maps, which was also consistent with our previous studies (Zhou et al., 2022; Zou et al., 2017; Zou et al., 2018).

2.3.2. Accuracy assessment

This study used confusion matrices to assess the accuracy of the water mapping method. Specifically, a total of 800 areas of interest (AOIs) with a radius of 100 m, covering more than 34,400 Landsat pixels, across the whole MP, were randomly generated for visual interpretation. The very high-resolution (VHR) satellite images from Centre National d'Etudes Spatiales (CNES)/Astrium at the platform of Google Earth Pro were used to interpret the types of AOIs. To ensure that the reference images are consistent with the resultant water body maps in time, we selected and interpreted the VHR images within the AOIs in the same year as the generated surface water body maps. The spatial distributions of the 800 AOIs (221 water AOIs and 579 non-water AOIs) were shown in Fig. 5. We calculated the overall accuracy of the water body maps for 1991, 2000, 2010, and 2020 by generating the confusion matrices using ENVI 5.6 platform, and found that the overall accuracy of the water body maps for the four years were 96.5 % (kappa coefficient of 0.92), 96.9 % (0.92), 96.3 % (0.90), and 97.9 % (0.95), respectively (Table 1). The above analyses indicated that the accuracy of these water body maps from our proposed method was reliable and could support the continuous monitoring of changes in SWA in the MP.

2.3.3. Analyses of spatial and temporal dynamics of SWA and TWS

We investigated the spatial and temporal changes in SWA and TWS at both the pixel and regional scales. Firstly, the pixels with water frequencies [75 %, 100 %] were considered year-long surface water bodies and marked as 1, while those below 75 % were considered seasonal water bodies or non-water and marked as 0. Based on the annual 30-m binary maps of year-long surface water bodies of the MP from 1991 to 2021 (Fig. 3), we aggregated them into 0.5 arc degrees to generate annual SWA percentage maps. Secondly, we applied the Theil-Sen slope estimator and Mann-Kendall test method to calculate the slope of annual SWA and statistical significance level for each pixel, to derive the

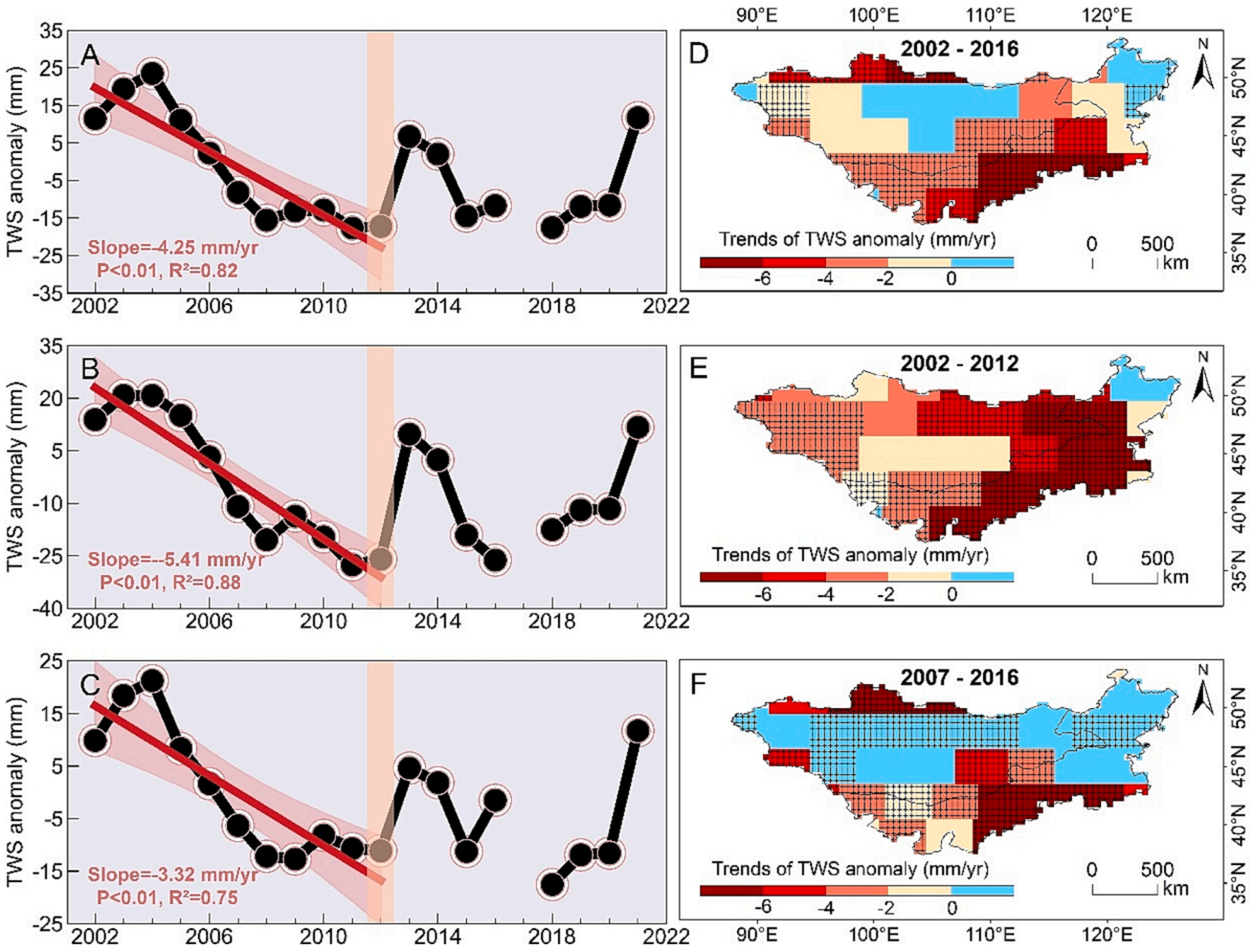

Fig. 9. Inter-annual variations and trends of TWS over the MP (A), Inner Mongolia (B), and Mongolia (C) from 2002 to 2016. Spatial change pattern of the TWS in MP from 2002 to 2016 (D), 2002 to 2011 (E), and 2007 to 2016 (F). The "+" symbol in each pixel indicated that the linear trends reached a statistical significance level of p-value < 0.05.

resultant map of linear trends of SWA. The Theil-Sen slope estimator has the advantages of high computation efficiency and insensitivity to measurement error and outlier data. The Mann-Kendall test method is a non-parametric test model, which does not require the measurement values to follow the normal distribution, nor does it require the changing trend to be linear. Most importantly, it is almost free from the influence of missing values and abnormal values (Matthias et al., 2015; Yang et al., 2019). Finally, we explored the inter-annual variability and linear trends of SWA in the MP at a regional scale based on Python 3.9 programming language. Similarly, we examined the inter-annual variability and linear trends of TWS, AP, and AMT at the pixel and regional scales.

2.3.4. *Driver analyses of SWA and TWS dynamics*

Previous researches (Tao et al., 2015; Zhang et al., 2017; Zhou et al., 2019) had recorded the shrinkage of surface water bodies in the MP since the early 1990s and attributed their drivers to intense human activities (i.e., coal mining, overgrazing, etc.), which were consistent with our current study. Considering that the most interesting finding in this paper was that SWA and TWS experienced significant recovery processes over the past decade following long-term shrinkage and depletion, here, we mainly focused on the driving factors of the recoveries of SWA and TWS. Based on the change analyses of SWA and TWS, we found that the increases of SWA in the MP over the past decade mainly happened in Inner Mongolia, and we identified two hotspots with the most rapid expansion of SWA. Firstly, for each hotspot, the timeline of the implementation of various ecological and environmental conservation policies was generated, and the inflection points of inter-annual variations of SWA and TWS were matched with the times of the implementation of major policies and regulations. Secondly, in view of the fact that ecological protection efforts would directly affect soil erosion areas in such an ecologically sensitive region, we investigated the changes in soil erosion treatment areas in each hotspot and analyzed the correlation between SWA and the areas of soil erosion treatment. Annual areas of soil erosion treatment were derived from the *Bulletin of Soil and Water Conservation* (https://slt.nmg.gov.cn/) issued by the Water Conservancy Department of Inner Mongolia. Finally, we applied the partial correlation model to quantitatively analyze the effects of each driving factor on SWA changes, in which AP and AMT were used to measure climate change, while the soil erosion treatment areas were selected as the index to reflect the influences from human activities.

3. Results

3.1. *Inter-annual variations and trends of SWA from 1991 to 2021*

Overall, MP experienced a considerable decline in SWA (-205.92 km^2/yr) before 2009 while continuous increases with a rate of 85.50 km^2/yr after that (Fig. 6A), in which Inner Mongolia dominated the trends of changes in SWA in the MP. Specifically, although the inter-annual variations and trends of SWA in Inner Mongolia were similar

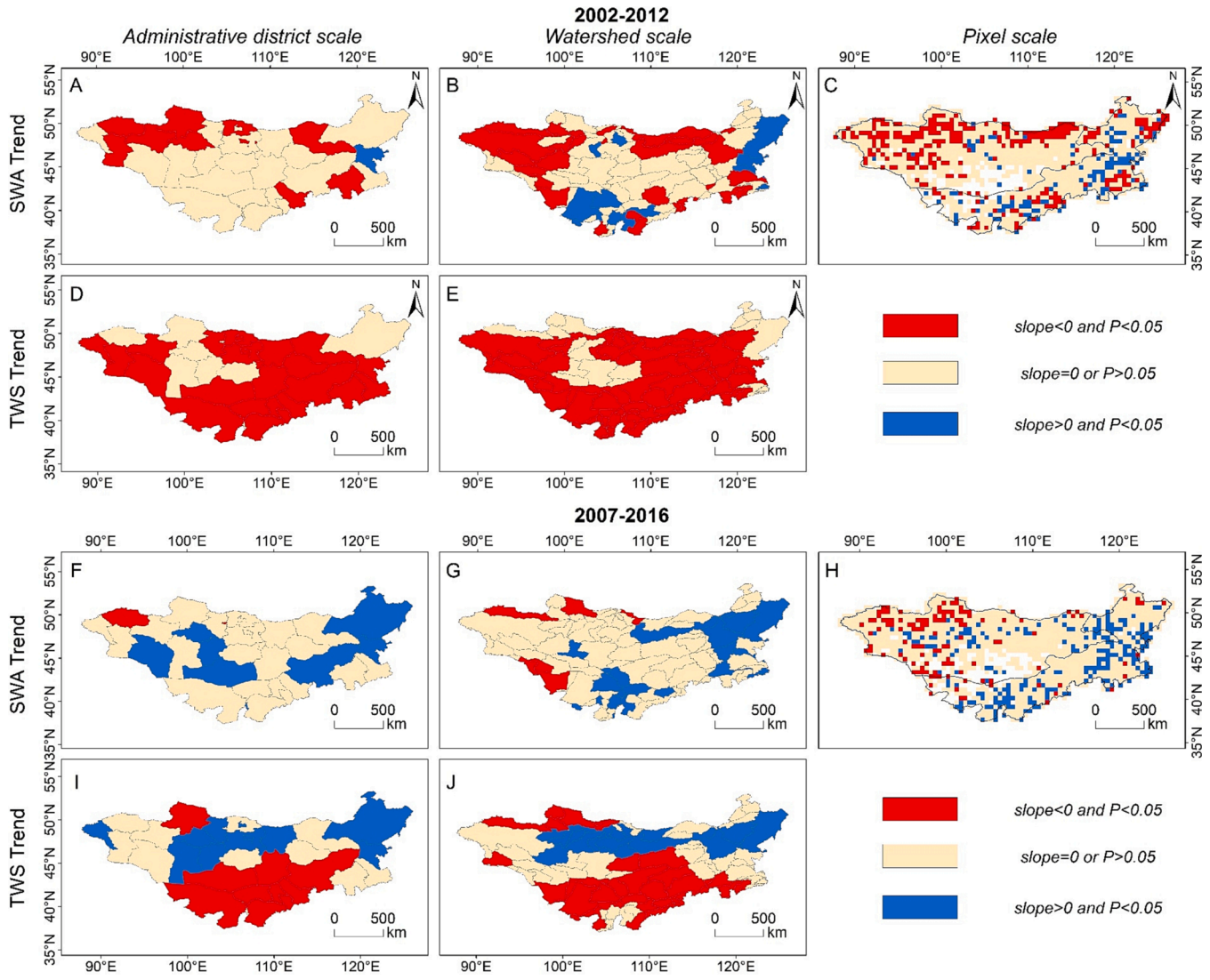

Fig. 10. Inter-annual variations and trends of SWA and TWS at different spatial scales.

to those of Mongolia (Fig. 6A and B), the decreasing rate of SWA was higher in Inner Mongolia (-117.51 km^2/yr) compared with Mongolia (-88.31 km^2/yr), agreeing well with previous studies (Tao et al., 2015; Zhou et al., 2019). In addition, we found an interesting phenomenon that Inner Mongolia also dominated the increases in SWA in the MP in the past decade. From 2009 to 2021, SWA showed a significantly ($p < 0.01$) and continuously increasing trend in Inner Mongolia, from -857.05 km^2/yr to 273.62 km^2/yr, at a rate of 72.21 km^2/yr. However, the rate of changes in SWA in Mongolia was much smaller, and the trend was not statistically significant (13.30 km^2/yr, $p = 0.18$). To explore the dynamics of surface water bodies with different sizes, we divided the surface water bodies on the MP into two categories of small (<1 km^2) and large (≥1 km^2) ones, and investigated the inter-annual variations and trends of their areas from 1991 to 2021 (Fig. 7). We found that SWA changes in Inner Mongolia were dominated by large water bodies (-91.15 km^2/yr from 1991 to 2009 and 61.61 km^2/yr from 2009 to 2021) (Fig. 7 B and E), while those in Mongolia were dominated by small ones (-46.96 km^2/yr from 1991 to 2009 and 8.83 km^2/yr from 2009 to 2021) (Fig. 7 C and F), no matter for the first period with surface water shrinkage or the last period with surface water expansion.

By examining the spatial patterns of linear trends of SWA, we found that the number of pixels with significantly decreasing trends (161) of SWA was more than that with increasing trends (598) from 1991 to 2021 (Fig. 6D). However, when we focused on different periods, the changes in SWA were mainly characterized by downward trends before 2009 (Fig. 6E), while they were mainly upward trends after 2009 (Fig. 6F). Specifically, among the 1421 0.5° × 0.5° pixels in the map of linear trends of SWA during 1991–2009, 618 pixels (43.49 %) experienced significantly decreasing trends in SWA while 154 pixels (10.83 %) experienced significantly increasing trends (Fig. 6E). From 2009 to 2021, the number of pixels experiencing increasing trends in SWA accounted for 54.40 % (773), in which the upward trends of SWA of 204 pixels were significant. However, only 112 pixels (7.88 %) experienced significantly decreasing trends in SWA (Fig. 6F). In addition, we found that the most rapid increases in SWA occurred in the southern parts (cities of Ordos, Bayannur, and Baotou) and northeastern parts (Hulunbuir City) of Inner Mongolia, which were the two hotspots of SWA recovery identified in this study (Fig. 6F).

At the administrative district scale (prefectural level for Inner Mongolia and provincial level for Mongolia), we found that the spatial distributions of surface water resources were uneven in the MP (Fig. 8A). Overall, SWA was the largest in the western parts of the plateau where many famous lakes (e.g., Lake Uvs and Lake Hovsgol, etc.) gather, followed by the eastern and central parts. The average annual SWA (ha) per unit land area (km^2) in a district during 1991–2021 varied from 0.003 ha/km^2 in Omnogovi Province to 6.6 ha/km^2 in Uvs Province in

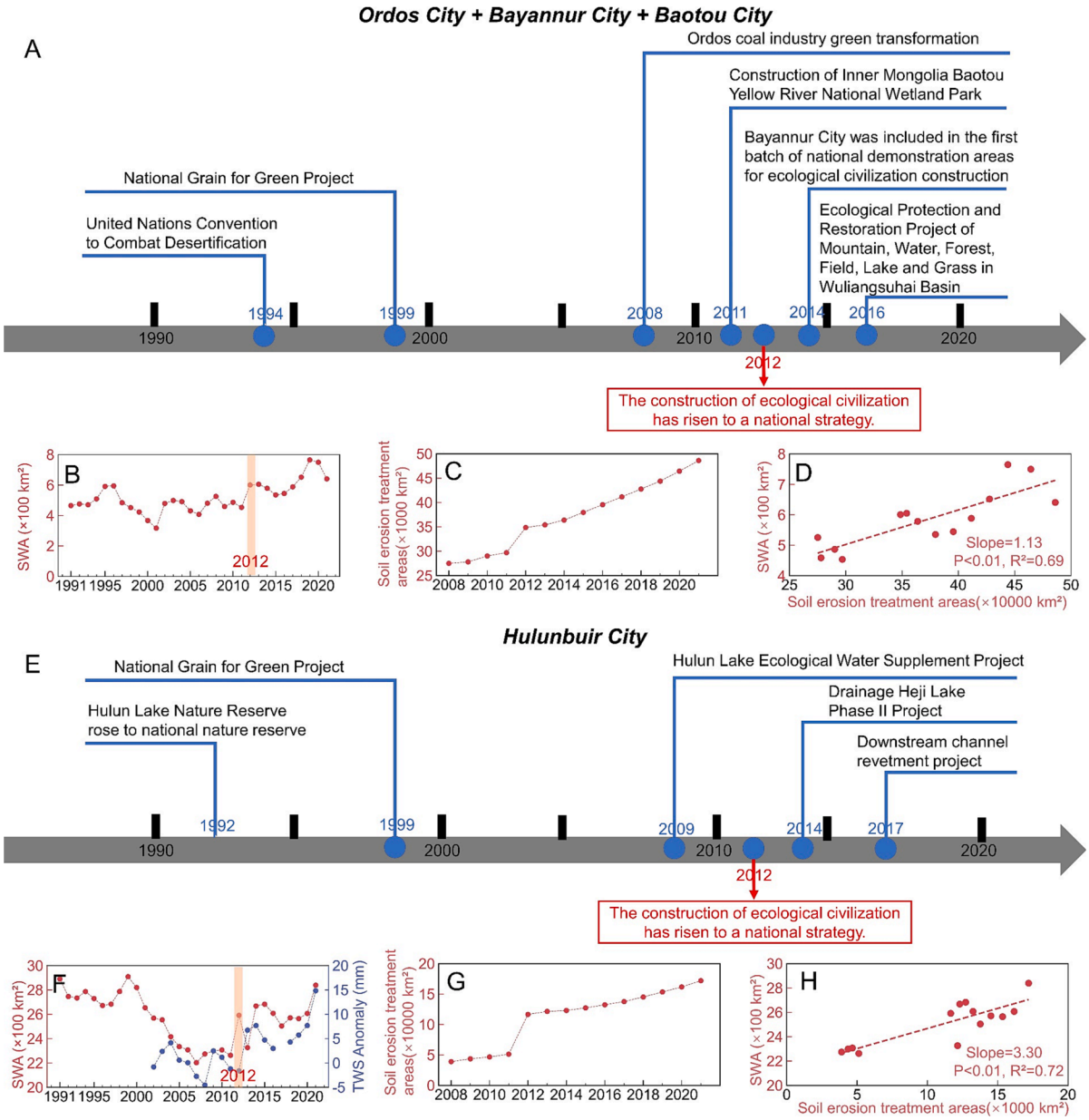

Fig. 11. Timelines of major ecological protection policies and the responses of inter-annual variations of SWA and TWS on them. (A) Retrieved major ecological protection policies in the cities of Ordos, Bayannur, and Baotou since 1990; Inter-annual variations of SWA (B) and the areas of soil erosion treatment (C); (D) Linear trends between SWA and the areas of soil erosion treatment; (E) Retrieved major ecological protection policies in Hulunbuir City since 1990; Inter-annual variations of SWA (F) and the areas of soil erosion treatment (G); (H) Linear trends between SWA and the areas of soil erosion treatment.

Mongolia. The standard deviation of SWA per unit land area in a district ranged between 0.004 ha/km^2 in Dornogovi Province in Mongolia and 1.05 ha/km^2 in Wuhai City in Inner Mongolia. Inter-annual changes in SWA in the MP during 1991–2021 showed divergent trends. Among the 34 administrative districts in the MP, 22 districts experienced significantly downward trends of SWA, ranging from −19.17 km^2/yr in Xilin Gol League in Inner Mongolia to −0.06 km^2/yr in Ulaanbaatar in Mongolia. Only 6 districts located in the southern parts of Inner Mongolia underwent significant increases in SWA, namely: Erdos, Byannur, Hohhot, Baotou, Wuhai, and Alxa League which included one of the two hotspots of SWA recovery identified in this study (Ordos City + Bayannur City + Baotou City). However, when we focused on the trends of SWA in different periods, the clearly contrary trends of SWA before and after 2009 could also be found. From 1991 to 2009, 20 districts experienced significantly decreasing trends of SWA, with which the most rapid decline of SWA occurred in Hulunbuir City of Inner Mongolia (Fig. 8C and D); while only 13 districts underwent significantly increasing trends. (Fig. 8C and D). Conversely, SWA showed significantly increasing trends in 10 districts from 2009 to 2021, with the most rapid increase of SWA in Hulunbuir City, too (Fig. 8E and F). And no administrative region showed a significant downward trend.

3.2. Inter-annual variations and trends of TWS from 2002 to 2021

Similar to the variations of SWA, TWS in the MP had undergone two stages of changes, namely: continuous and significant decline before 2012 and fluctuating rebound after that (Fig. 9A-C). For the first phase, TWS significantly ($p < 0.01$) and continuously decreased in the entire MP, Inner Mongolia, and Mongolia, with rates of −4.25 mm/yr, −5.41 mm/yr, and −3.32 mm/yr, respectively. The decreasing trends of TWS had been alleviated in the MP since 2012. Although TWS decreased again after 2013, there was a continuous and sharp increase in TWS

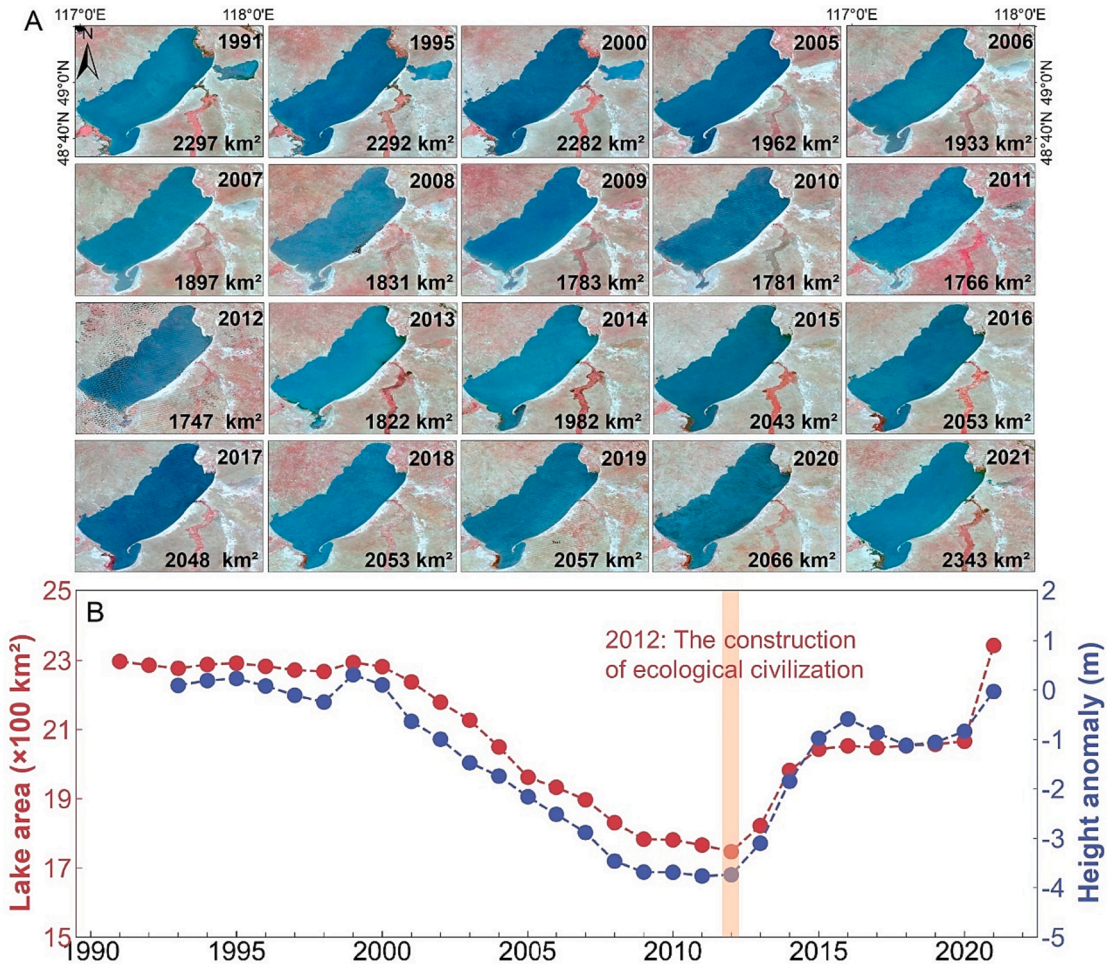

Fig. 12. Changes in surface water of Lake Hulun. (A) Annual surface water extents of Lake Hulun from 1991 to 2021, represented by Landsat image composite using the three bands of NIR, Red, and Green. (B) Inter-annual variations of water area and height of Lake Hulun. (For interpretation of the references to colour in this figure legend, the reader is referred to the web version of this article.)

during 2018–2021 (MP: from −1.76 mm to 1.17 mm; Inner Mongolia: from −2.96 mm to 0.78 mm; Mongolia: from −0.90 mm to 1.46 mm;), in which the value of 2021 was higher than that of 2013 and rebounded to the level around 2005 (Fig. 9A-C).

To have a better understanding of the spatial variability of TWS changes in the MP, we investigated the spatial patterns of linear trends of TWS during 2002–2016 (Fig. 9 D-F). We found that among the 1269 pixels with a grid size of 0.5 × 0.5 arc degree, there were 653 pixels (51.46 %) experiencing significant declines in TWS, mainly located in the southern parts of the MP (i.e., Inner Mongolia). In addition, the regions with the most rapid loss of TWS occurred in the southern parts of Inner Mongolia, covering 126 pixels (Fig. 9D). However, the spatial patterns of linear trends of TWS greatly varied in different periods. Similarly, we chose 2002–2012 as the first phase of TWS changes (Fig. 9E). The results showed that the number of GRACE pixels with significant declines in TWS increased to 895 (70.53 %), while no pixel experienced significant increases in TWS. Compared with the results of 2002–2016, those new pixels with significant loss of TWS during 2002–2012 were mainly concentrated in the eastern, northern, and western parts of the MP. In addition, the regions with the most serious loss of TWS expanded northward to Xilin Gol League and Hulunbuir City in Inner Mongolia, and Dornod Aymag in Mongolia. Conversely, the loss of TWS has been widely alleviated during the second phase of 2007–2016 (Fig. 9F). The reason why we extended the start year period to 2007 was to ensure the reliability of statistical analyses with at least ten samples. We found that there were 714 pixels with TWS increases, in which 351 pixels experienced significant upward trends in TWS, mainly concentrated in the northern part of the MP. However, among these 1269 pixels, 484 of them experienced significantly downward trends of TWS during 2007–2016. It was notable that Hulunbuir City experienced a significant recovery of TWS in the later period, which was also one of the hotspots of SWA increases in this study.

To further reveal the recovery of SWA and TWS in the MP during the later period (since ~ 2010) compared with the former one (before ~ 2010), we investigated the spatial patterns of changing trends of SWA and TWS during 2002–2012 and 2007–2016 at the scales of an administrative region, watershed, and pixel (0.5° × 0.5°) (Fig. 10). From 2002 to 2012, there were 10 administrative regions (or 34 watersheds and 295 pixels) experiencing significant decreases in SWA, whereas SWA significantly increased in only 1 region (or 13 watersheds and 95 pixels) (Fig. 10A-C). Conversely, SWA showed significantly and continuously increasing trends in 8 regions (or 24 watersheds and 215 pixels) during 2007–2016 (Fig. 10F-H); while only 2 regions (or 8 watersheds and 122 pixels) experienced significant decreases in SWA. Similarly, we found that among the 34 administrative regions (or 117 watersheds) in the MP, 25 regions (or 85 watersheds) experienced significantly downward trends of TWS during 2002–2012, while no region and watershed experienced increases in TWS (Fig. 10D-E). However, TWS showed significantly increasing trends in 12 regions (or 21 watersheds) which were mainly located in the northern parts of the plateau during the period (Fig. 10I-J). All these comparisons and analyses suggested the remarkable recovery of SWA and TWS in the MP during the past decade.

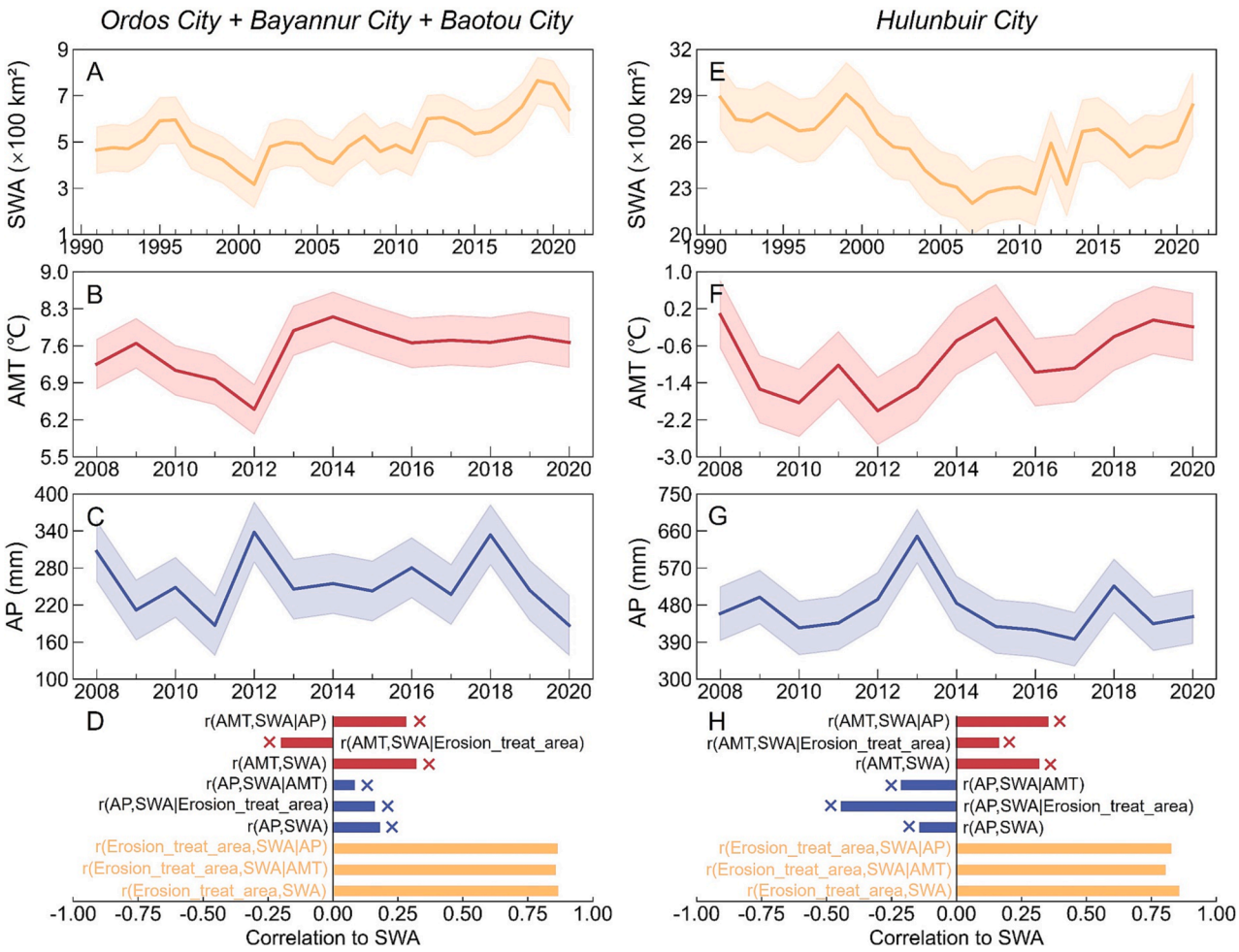

Fig. 13. The time series of SWA in the first hotspot (A).Inter-annual variations of AMT (B) and AP (C) in the first hotspot (Ordos City + Bayannur City + Baotou City) from 1991 to 2020. Correlation and partial correlations between anthropogenic or climatic factors and SWA change in the first hotspot (D). Shown in orange, from bottom to top, is first the correlation between soil erosion treatment area (Erosion_treat_area) and SWA, followed by partial correlation r between Erosion_treat_area and SWA after controlling for the effect of AMT and AP. Shown in blue, from bottom to top, is first the correlation between AP and SWA, followed by partial correlations r between AP and SWA after controlling for the effect of Erosion_treat_area and AMT. Shown in red, from bottom to top, is first the correlation between AMT and SWA, followed by partial correlations r between AMT and SWA after controlling for the effect of Erosion_treat_area and AP. Each cross symbol indicates that the trend was not statistically significant ($p \geq 0.05$). The time series of SWA in the second hotspot (E). Inter-annual variations of AMT (F) and AP (G) in the second hotspot (Hulunbuir City) from 1991 to 2020. Correlation and partial correlations between anthropogenic or climatic factors and SWA changes in the second hotspot which was similar to D (H). (For interpretation of the references to colour in this figure legend, the reader is referred to the web version of this article.)

3.3. ·Drivers of the recoveries of SWA and TWS

Previous·studies·(Tao et al., 2015; Zhang et al., 2017; Zhou et al., 2019) had documented the rapid shrinkage of widely distributed lakes in the MP before 2010 and attributed their drivers to intense human activities (i.e., coal mining, overgrazing, etc.), which further proved the reliability of our current findings that SWA showed significantly and continuously decreasing trends before 2009. Moreover, the most interesting finding in this study was that SWA and TWS experienced remarkable recoveries over the past decade following long-term shrinkage and depletion. Therefore, here, we mainly focused on the driving factors of the recoveries of SWA and TWS in the later period. Considering that Inner Mongolia dominated the raise of SWA in the MP after 2009, in which the two hotspots with the most rapid expansion of surface water bodies were identified in the southern (Ordos City + Bayannur City + Baotou City) and northeastern (Hulunbuir City) parts, we quantitatively analyzed the driving factors of SWA increases in the two hotspots from the aspects of climate change and human activities.

The southern parts of Inner Mongolia were the regions with serious desertification and soil erosion. Therefore, a series of key ecological restoration projects have been developed and implemented since the 1990 s (e.g., returning farmland to forestland and grassland since 1999). Other important ecological projects implemented in the regions have been listed in Fig. 11A. Especially, China launched the construction of ecological civilization and rose it to a national strategy since 2012, greatly contributing to ecological environment treatment and the following restoration of wetlands and lakes (Fig. 11A). Fig. 11B showed the remarkable increases of SWA in the three administrative regions since 2012. Considering that soil erosion could significantly affect the changes in the spatial extents of surface water bodies (Wu et al., 2020), here, we selected the areas of soil erosion treatment as the major index to reflect the effects of ecological restoration efforts. In addition, we chose AP and AMT as indicators to measure climate change. Firstly, we found that annual areas of soil erosion treatment continuously increased since 2008 (Fig. 11C). Correlation analysis suggested that SWA was significantly ($p < 0.01$, $R^2 = 0.69$) and positively correlated with the areas of soil erosion treatment (Fig. 11D). Secondly, the trends of AP and AMT were not obvious in these regions since 2008 (Fig. 13B and C), which suggested that climate change could not be the major drivers of SWA expansion. Thirdly, we found that interannual variations and

trends of SWA were not consistent with that of AP/AMT (Fig. 13A-C), and the correlation between SWA and AP/AMT was also not statistically significant (Fig. 13D). In addition, for the significant and positive correlation between SWA and the areas of soil erosion treatment, its correlation coefficient was still significant after adding AP or AMT to the partial correlation model. All these statistical analyses have proved that soil erosion treatment due to the implementation of ecological projects was of great significance to the recovery of SWA over the last decade.

Similar to the southern parts of Inner Mongolia, Hulunbuir City had also experienced some major ecological restoration projects in the past years, such as the ecological water compensation project in 2009 and the construction of ecological civilization in 2012 (Fig. 11E). While SWA continuously decreased before 2012, we found that there was a rapid recovery process for SWA in the Hulunbuir City in the past decade (Fig. 10F). Taking Lake Hulun as an example, we found that the lake area continuously decreased before 2012 and then obviously increased (Fig. 12), which was highly consistent with the finding in previous study that the water level and storage of the lake experienced significant increasing trends after the continuous decline before 2012 (Fan et al., 2021). The originally dried-up water bodies in the southern and northeastern parts of Lake Hulun had gradually reappeared in people's vision since 2012 (Fig. 12A). In addition, by utilizing lake surface height data, it was found that the inter-annual variations of SWA and water surface height were highly consistent with each other (Fig. 12B), which further validated the reliability of SWA change surveys in this study.

In terms of the quantitative driver analyses of SWA changes in Hulunbuir City, the areas of soil erosion treatment were also selected to reflect the achievements of ecological protection, while AP and AMT were considered climate change factors. Firstly, a continuously increasing trend was observed for the areas of soil erosion treatment (Fig. 11G). Correlation analysis also showed a significant ($p < 0.01$, $R^2 = 0.72$) and positive correlation between the areas of surface water bodies and the soil erosion treatment areas (Fig. 11H). Secondly, the changing trends of AP and AMT were not consistent with that of SWA (Fig. 13E-G), and their correlations with SWA were also not statistically significant (Fig. 13H). Finally, after adding the influence of AMT or AP to the partial correlation model, the correlation coefficients between SWA and the areas of soil erosion treatment were still statistically significant (Fig. 13H). Therefore, it could be concluded that the ecological protection achievements of Hulunbuir City were remarkable and significantly contributed to the increases of SWA and following recovery of TWS in the region. Considering that the two hotspots showed significant and positive correlations between SWA and ecological restoration efforts, it could further support our view by comparing with the correlations in the regions where did not experience significant increases of SWA. By selecting two administrative regions (i.e., provinces of Dornod and Bayankhongor) in Mongolia where did not experience significant increases of SWA to conduct the controlled experiment, we found that the trends of SWA and ecological restoration efforts were not consistent with each other and their correlations were not statistically significant in these two regions (see Text S1 and S2, Figs. S1 and S2 for detailed information). All these statistical analyses proved that ecological restoration efforts in typical regions (e.g., Hulunbuir in Inner Mongolia) greatly contributed to the local SWA recovery.

4. Discussion

4.1. Implications of SWA and TWS recovery in the MP

As one of the famous plateaus in Asia, the MP plays a vital role in regulating climate in northern Asia (Liu et al., 2013; Luo et al., 2021; Zhang et al., 2020b). The plateau possesses a large number of surface water bodies (e.g., lakes and wetlands) with different sizes, which are of great significance to ensuring human livelihood and industrial and agricultural production, as well as maintaining the stability of the ecosystem (Bai et al., 2021). However, due to the intense human disturbance (i.e., coal mining, overgrazing, etc.), the MP experienced rapid and continuous shrinkages of surface water bodies since the start of the 1990s, which has been proved by previous research and our current study (Tao et al., 2015; Zhou et al., 2019). In addition, the deterioration and decline of surface water bodies were more serious in Inner Mongolia compared to that in Mongolia. The lake shrinkage brought considerable threats to the regional environment and ecosystems, including dust release, water salinization, and waterfowl decline (Yafeng and Jiawen, 1990). To our joy, we found that the MP was experiencing a remarkable process of water resources recovery in the past decade, which was reflected in the significant and continuous increases of the SWA and TWS. The current study found that a series of national ecological restoration projects were the main driving factors to the rapid expansion of SWA in Inner Mongolia (Fu et al., 2023; Li et al., 2020b). The significant recovery of water resources such as the expansion of the wetlands and lakes, provided a good growth substrate for aquatic plants and attracted a large number of organisms as habitats, which was of positive significance for enriching the diversity of local organisms and maintaining the stability of the ecological environment in the region (Mitsch et al., 2013).

4.2. Comparison with previous researches

Previous researches had focused on analyzing the changes in the numbers and areas of lakes greater than 1 km^2 in the MP and conducted a quantitative analysis of the driving factors affecting the changes of these lakes (Tao et al., 2015; Zhang et al., 2017; Zhou et al., 2019). In this study, we expanded the monitoring targets to all these surface water bodies with sizes greater than or equal to 30 m × 30 m, and reveal that SWA changes were dominated by large water bodies in Inner Mongolia while small ones in Mongolia. Previous researches mainly reported the rapid shrinkage of these widely distributed lakes due to intense human activities such as coal mining and overgrazing (Tao et al., 2015; Zhang et al., 2017). Here, using all the available Landsat SR observations and the GEE cloud computing platform, we investigated the spatial and temporal changes of SWA at inter-annual scale and found the remarkable increases (85.50 km^2/yr) of surface water bodies in the study area during the past decade induced by ecological restoration efforts following the long-term continuous shrinkages (−205.9 km^2/yr).

Quantifying and comparing the changing trends of SWA and TWS can contribute to a deeper understanding of the feedback of the dynamics of surface water bodies to regional water resources. Considering that surface water is one of the important components of TWS (36.08 ± 9.89 %) (Wang et al., 2020), the dynamics of surface water bodies always play an important role in affecting the changes in TWS to a certain extent. For example, the increase of surface water is conducive to the recharge of groundwater, which will drive the following increases in TWS (Thomas et al., 2017). However, to date, few studies have systematically quantified the spatial and temporal changes of SWA and TWS and analyzed their interconnections. With the help of GRACE and GRACE-FO mascon data sets, we examined the changes in TWS in the MP from 2002 to 2021, and found that the loss of TWS also have been alleviated over the past decade. In addition, in the current study, we identified Hulunbuir City as a typical region where experienced both increases in SWA and TWS in the past decade, suggesting that the expanding surface water bodies had a positive feedback on TWS. Finally, we qualitatively and quantitatively attributed the drivers of recoveries of SWA and TWS in the MP during the past decade to ecological restoration efforts in China. Therefore, this study not only reported the severe shrinkage of surface water bodies in the MP since the early 1990s, which was consistent with previous studies (Tao et al., 2015; Zhang et al., 2017; Zhou et al., 2019), but also revealed the improvement of surface and terrestrial water resources induced by various ecological restoration efforts in China in the past decade.

4.3. Uncertainties and limitations in this study

Together with previous researches (Pekel et al., 2016; Song et al., 2018; Wang et al., 2020; Zhou et al., 2022), the continuous monitoring of SWA and TWS changes and the quantitative driver analyses in this study significantly contributed to the understanding of water resource status in the MP and promoted the practice for sustainable water management and protection. However, we have to realize that there were still some uncertainties and limitations remained regarding to the data and methodologies used, which need to be improved in future studies. First of all, we used Landsat SR data with a spatial resolution of 30 m to annually map and detect the changes in surface water bodies, which significantly improved the accuracy compared to the researches that investigated the dynamics of SWA using MODIS data (Ji et al., 2018). However, those water bodies with sizes smaller than 30 m × 30 m, which were also important components of surface water resources and played a key role in regulating regional climate, might be neglected and missed. Secondly, despite that the pixels of snow, clouds, cloud shadows, and terrain shadows have been removed in remote sensing data preprocessing procedures, some bad-quality Landsat observations might still remain and could cause low-frequency noises in water frequency maps to a certain degree. However, what we focused on in this study were those pixels with water occurrence frequencies equal to or greater than 0.75, which could avoid the disturbance of low-frequency data noises. Finally, there will inevitably be differences between the results of remote sensing modeling and in-situ measurements regarding to temperature and precipitation. Therefore, we used two kinds of global climate data sets to depict the changing trends of AP and AMT to reduce the uncertainties of data.

5. Conclusion

Water resources are extremely critical for ensuring human livelihood and agricultural and industrial production, as well as maintaining regional ecosystem stability and achieving SDGs in the MP. Using all those good-quality Landsat observations, a robust water mapping algorithm based on water and vegetation indices and thresholds, and GEE cloud computing platform, we generated the annual maps of year-long surface water bodies with a spatial resolution of 30 m and depicted the complete changing processes of SWA in the MP during 1991–2021. In addition, using the monthly GRACE and GRACE-FO mascon data products with a spatial resolution of 0.5° produced by NASA JPL, we investigated the inter-annual variations and trends of TWS from 2002 to 2021. We found that the MP experienced remarkable increases (85.50 km^2/yr) in SWA since 2009 after continuous surface water shrinkage (-205.92 km^2/yr) for over 20 years, in which Inner Mongolia played a dominant role in the recovery of SWA (72.21 km^2/yr). Similarly, TWS had undergone continuous decline before 2012 (MP: −4.25 mm/yr; Inner Mongolia: −5.41 mm/yr; Mongolia: −3.32 mm/yr) and fluctuating rebound after that (MP: −1.72 mm/yr to 1.17 mm/yr; Inner Mongolia: −2.62 mm/yr to 0.78 mm/yr; Mongolia: −0.15 mm/yr to 1.46 mm/yr). The most significant recovery of TWS mainly happened in the northern part of the MP. Both qualitative and quantitative attribution analyses showed that the key ecological restoration projects in China, especially the construction of ecological civilization since 2012, were the major drivers for the recovery of surface and terrestrial water resources. While previous studies reported the considerable decline of surface water resources induced by human activities in the MP since the 1990s, our research provided gratifying satellite evidence for the significant recoveries of surface and terrestrial water resources in the plateau during the past decade under the influence of ecological restoration efforts.

CRediT authorship contribution statement

Zhenfei Gao: Methodology, Formal analysis, Writing – original draft. **Yan Zhou:** Supervision, Conceptualization, Writing – review & editing. **Yaoping Cui:** Supervision, Conceptualization, Writing – review & editing. **Jinwei Dong:** Data curation, Writing – review & editing. **Xinxin Wang:** Data curation, Writing – review & editing. **Guosong Zhao:** Writing – review & editing. **Zhenhua Zou:** Writing – review & editing. **Xiangming Xiao:** Writing – review & editing.

Declaration of Competing Interest

The authors declare that they have no known competing financial interests or personal relationships that could have appeared to influence the work reported in this paper.

Data availability

Data will be made available on request.

Acknowledgments

This study is supported by the National Natural Science Foundation of China (42301125, 42071415), the China Postdoctoral Science Foundation (2022M721005), and the Opening Foundation of Henan Key Laboratory of Ecological Environment Protection of Yellow River Basin (LYBEPR202303).

Appendix A. Supplementary data

Supplementary data to this article can be found online at https://doi.org/10.1016/j.ecolind.2023.111193.

References

Abatzoglou, J.T., Dobrowski, S.Z., Parks, S.A., et al., 2018. TerraClimate, a high-resolution global dataset of monthly climate and climatic water balance from 1958–2015. Sci. Data 5, 170191.
Amani, M., Ghorbanian, A., Ahmadi, S.A., et al., 2020. Google Earth Engine Cloud Computing Platform for Remote Sensing Big Data Applications: A Comprehensive Review. IEEE J. Sel. Top. Appl. Earth Obs. Remote Sens. 13, 5326–5350.
Bai, M., Mo, X., Liu, S., et al., 2021. Detection and attribution of lake water loss in the semi-arid Mongolian Plateau—A case study in the Lake Dalinor. Ecohydrology 14, e2251.
Bao, G., Chen, J., Chopping, M., et al., 2019. Dynamics of net primary productivity on the Mongolian Plateau: Joint regulations of phenology and drought. Int. J. Appl. Earth Obs. Geoinf. 81, 85–97.
Bian, J., Li, A., Lei, G., et al., 2020. Global high-resolution mountain green cover index mapping based on Landsat images and Google Earth Engine. ISPRS J. Photogramm. Remote Sens. 162, 63–76.
Chambers, D.P., Bonin, J.A., 2012. Evaluation of Release-05 GRACE time-variable gravity coefficients over the ocean. Ocean Sci. 8, 859–868.
Chambers, P.D., Willis, et al., 2010. A Global Evaluation of Ocean Bottom Pressure from GRACE, OMCT, and Steric-Corrected Altimetry. J. Atmos. Oceanic Tech. 27, 1395–1402.
Chen, Z., Zhao, S., 2022. Automatic monitoring of surface water dynamics using Sentinel-1 and Sentinel-2 data with Google Earth Engine. Int. J. Appl. Earth Obs. Geoinf. 113, 103010.
Dong, J., Xiao, X., Menarguez, M.A., et al., 2016. Mapping paddy rice planting area in northeastern Asia with Landsat 8 images, phenology-based algorithm and Google Earth Engine. Remote Sens. Environ. 185, 142–154.
Duan, Y., Li, X., Zhang, L., et al., 2020. Mapping national-scale aquaculture ponds based on the Google Earth Engine in the Chinese coastal zone. Aquaculture 520, 734666.
Fan, C., Song, C., Liu, K., et al., 2021. Century-Scale Reconstruction of Water Storage Changes of the Largest Lake in the Inner Mongolia Plateau Using a Machine Learning Approach. Water Resour. Res. 57 e2020WR028831.
Foga, S., Scaramuzza, P.L., Guo, S., et al., 2017. Cloud detection algorithm comparison and validation for operational Landsat data products. Remote Sens. Environ. 194, 379–390.
Fu, B., Liu, Y., Meadows, M.E., 2023. Ecological restoration for sustainable development in China. Natl. Sci. Rev. 10, nwad033.
Getirana, A., Kumar, S., Girotto, M., et al., 2017. Rivers and Floodplains as Key Components of Global Terrestrial Water Storage Variability. Geophys. Res. Lett. 44, 10,359–310,368.
Gorelick, N., Hancher, M., Dixon, M., et al., 2017. Google Earth Engine: Planetary-scale geospatial analysis for everyone. Remote Sens. Environ. 202, 18–27.
Harris, I., Osborn, T.J., Jones, P., et al., 2020. Version 4 of the CRU TS monthly high-resolution gridded multivariate climate dataset. Sci. Data 7, 109.

Hongyuan, S., Xuefeng, C., Qingjie, L., et al., 2021. Evaluating the Accuracy of ERA5 Wave Reanalysis in the Water Around China. J. Ocean Univ. China 20, 1–9.
Huang, C., Chen, Y., Zhang, S., et al., 2018. Detecting, Extracting, and Monitoring Surface Water From Space Using Optical Sensors: A Review. Rev. Geophys. 56, 333–360.
Ji, L., Gong, P., Wang, J., et al. (2018). Construction of the 500-m Resolution Daily Global Surface Water Change Database (2001–2016). *Water Resour. Res., 54*, 10,270-210,292.
John, R., Chen, J., Ou-Yang, Z.-T., et al., 2013. Vegetation response to extreme climate events on the Mongolian Plateau from 2000 to 2010. Environ. Res. Lett. 8, 035033.
Johnson, D.M., 2019. Using the Landsat archive to map crop cover history across the United States. Remote Sens. Environ. 232, 111286.
Jun, C., Ban, Y., Li, S., 2014. Open access to Earth land-cover map. Nature 514, 434.
Lehner, B., Grill, G., 2013. Global river hydrography and network routing: baseline data and new approaches to study the world's large river systems. Hydrol. Process. 27, 2171–2186.
Li, F., Kusche, J., Rietbroek, R., et al. (2020a). Comparison of Data-Driven Techniques to Reconstruct (1992–2002) and Predict (2017–2018) GRACE-Like Gridded Total Water Storage Changes Using Climate Inputs. *Water Resources Research, 56*, e2019WR026551.
Liu, X., Hu, G., Chen, Y., et al., 2018. High-resolution multi-temporal mapping of global urban land using Landsat images based on the Google Earth Engine Platform. Remote Sens. Environ. 209, 227–239.
Li, Z., Ning, K., Chen, J., et al., 2020b. Soil and water conservation effects driven by the implementation of ecological restoration projects: Evidence from the red soil hilly region of China in the last three decades. J. Clean. Prod. 260, 121109.
Liu, X., Bao, S., Meng, F., 2022a. Inner Mongolia Water Footprint Account Accounting and Water Resources Evaluation Analysis. Acad. J. Environ. Earth Sci. 4.
Liu, X., Quan, L., Shan, Y., et al., 2022b. Exploring grassland ecosystem water use efficiency using indicators of precipitation and soil moisture across the Mongolian Plateau. Ecol. Ind. 142, 109207.
Liu, Y., Zhuang, Q., Chen, M., et al., 2013. Response of evapotranspiration and water availability to changing climate and land cover on the Mongolian Plateau during the 21st century. Global Planet. Change 108, 85–99.
Loveland, T.R., Dwyer, J.L., 2012. Landsat: Building a strong future. Remote Sens. Environ. 122, 22–29.
Luo, M., Meng, F., Sa, C., et al., 2021. Response of vegetation phenology to soil moisture dynamics in the Mongolian Plateau. Catena 206, 105505.
Ma, R., Duan, H., Hu, C., et al., 2010. A half-century of changes in China's lakes: Global warming or human influence? Geophys. Res. Lett. 37.
Matthias, F., Mirco, M., Kirsten, T., et al., 2015. Codominant water control on global interannual variability and trends in land surface phenology and greenness. Glob. Chang. Biol. 21, 3414–3435.
Mitsch, W.J., Bernal, B., Nahlik, A.M., et al., 2013. Wetlands, carbon, and climate change. Landsc. Ecol. 28, 583–597.
Pekel, J.-F., Cottam, A., Gorelick, N., et al., 2016. High-resolution mapping of global surface water and its long-term changes. Nature 540, 418–422.
Pokhrel, Y., Felfelani, F., Satoh, Y., et al., 2021. Global terrestrial water storage and drought severity under climate change. Nat. Clim. Chang. 11, 226–233.
Qiang, X., Yang, X., Ying, L., et al., 2019. Effects of afforestation on water resource variations in the Inner Mongolian Plateau. PeerJ 7, e7525.
Song, C., Ke, L., Pan, H., et al., 2018. Long-term surface water changes and driving cause in Xiong'an, China: from dense Landsat time series images and synthetic analysis. Sci. Bull. 63, 708–716.
Tamiminia, H., Salehi, B., Mahdianpari, M., et al., 2020. Google Earth Engine for geo-big data applications: A meta-analysis and systematic review. ISPRS J. Photogramm. Remote Sens. 164, 152–170.
Tao, S., Fang, J., Zhao, X., et al., 2015. Rapid loss of lakes on the Mongolian Plateau. Proc. Natl. Acad. Sci. 112, 2281–2286.
Thomas, B.F., Famiglietti, J.S., Landerer, F.W., et al., 2017. GRACE Groundwater Drought Index: Evaluation of California Central Valley groundwater drought. Remote Sens. Environ. 198, 384–392.
Verpoorter, C., Kutser, T., Seekell, D.A., et al., 2014. A global inventory of lakes based on high-resolution satellite imagery. Geophys. Res. Lett. 41, 6396–6402.
Wang, J., Song, C., Reager, J.T., et al., 2018. Recent global decline in endorheic basin water storages. Nat. Geosci. 11, 926–932.
Wang, X., Xiao, X., Zou, Z., et al., 2020. Gainers and losers of surface and terrestrial water resources in China during 1989–2016. Nat. Commun. 11, 3471.
Wang, X., Xiao, X., Xu, X., et al., 2021. Rebound in China's coastal wetlands following conservation and restoration. Nat. Sustainability 4, 1076–1083.
Wen, Z., Zhen, Z., Xiaobing, W., et al., 2022. Long-term spatiotemporal changes of surface water and its influencing factors in the mainstream of Han River China. J. Hydrol.: Regional Stud. 40, 101009.
Wu, Q., Ke, L., Wang, J., et al., 2023. Satellites reveal hotspots of global river extent change. Nat. Commun. 14, 1587.
Wu, G.-L., Liu, Y.-F., Cui, Z., et al., 2020. Trade-off between vegetation type, soil erosion control and surface water in global semi-arid regions: A meta-analysis. J. Appl. Ecol. 57, 875–885.
Wulder, M.A., White, J.C., Loveland, T.R., et al., 2016. The global Landsat archive: Status, consolidation, and direction. Remote Sens. Environ. 185, 271–283.
Yafeng, S., Jiawen, R., 1990. Glacier recession and lake shrinkage indicating a climatic warming and drying trend in central Asia. Ann. Glaciol. 14, 261–265.
Yamazaki, D., Trigg, M.A., Ikeshima, D., 2015. Development of a global ~90m water body map using multi-temporal Landsat images. Remote Sens. Environ. 171, 337–351.
Yang, J., Dong, J., Xiao, X., et al., 2019. Divergent shifts in peak photosynthesis timing of temperate and alpine grasslands in China. Remote Sens. Environ. 233, 111395.
Zhang, Y., Wang, Q., Wang, Z., et al., 2020b. Impact of human activities and climate change on the grassland dynamics under different regime policies in the Mongolian Plateau. Sci. Total Environ. 698, 134304.
Zhang, G., Yao, T., Piao, S., et al., 2017. Extensive and drastically different alpine lake changes on Asia's high plateaus during the past four decades. Geophys. Res. Lett. 44, 252–260.
Zhang, G., Yao, T., Xie, H., et al., 2020a. Response of Tibetan Plateau lakes to climate change: Trends, patterns, and mechanisms. Earth Sci. Rev. 208, 103269.
Zhao, M.A.G., Zhang, J., et al., 2021. Ecological restoration impact on total terrestrial water storage. Nat. Sustainability 4, 56–62.
Zhou, Y., Dong, J., Xiao, X., et al., 2019. Continuous monitoring of lake dynamics on the Mongolian Plateau using all available Landsat imagery and Google Earth Engine. Sci. Total Environ. 689, 366–380.
Zhou, Y., Dong, J., Cui, Y., et al., 2022. Rapid surface water expansion due to increasing artificial reservoirs and aquaculture ponds in North China Plain. J. Hydrol. 608, 127637.
Zhou, Y., Dong, J., Cui, Y., et al., 2023. Ecological restoration exacerbates the agriculture-induced water crisis in North China Region. Agric. For. Meteorol. 331, 109341.
Zhu, J., Song, C., Wang, J., et al., 2020. China's inland water dynamics: The significance of water body types. Proc. Natl. Acad. Sci. 117, 13876–13878.
Zhu, E., Wang, Y., Yuan, X., 2023. Changes of terrestrial water storage during 1981–2020 over China based on dynamic-machine learning model. J. Hydrol. 621, 129576.
Zhu, Z., Wulder, M.A., Roy, D.P., et al., 2019. Benefits of the free and open Landsat data policy. Remote Sens. Environ. 224, 382–385.
Zou, Z., Dong, J., Menarguez, M.A., et al., 2017. Continued decrease of open surface water body area in Oklahoma during 1984–2015. Sci. Total Environ. 595, 451–460.
Zou, Z., Xiao, X., Dong, J., et al., 2018. Divergent trends of open-surface water body area in the contiguous United States from 1984 to 2016. Proc. Natl. Acad. Sci. 115, 3810–3815.